NASA TECHNICAL MEMORANDUM

NASA TM X-52609

NASA TM X-52609

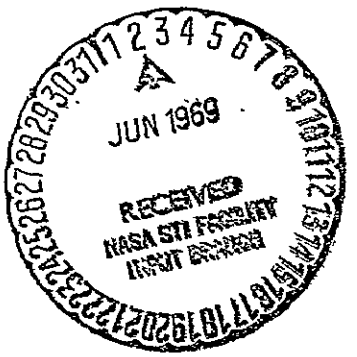

EFFECT OF A RECTANGULAR SIMULATED WING ON THE PRESSURE-DRAG COEFFICIENT OF VARIOUS BOAT-TAILS AT MACH NUMBERS FROM 0.60 TO 1.47

by Douglas E. Harrington
Lewis Research Center
Cleveland, Ohio
1969

"This information is being published in preliminary form in order to expedite its early release."

NASA TM X-52609

EFFECT OF A RECTANGULAR SIMULATED WING ON THE PRESSURE-DRAG COEFFICIENT OF VARIOUS BOAT-TAILS AT MACH NUMBERS FROM 0.60 TO 1.47

by Douglas E. Harrington

Lewis Research Center
Cleveland, Ohio

NATIONAL AERONAUTICS AND SPACE ADMINISTRATION

EFFECT OF A RECTANGULAR SIMULATED WING ON THE PRESSURE-DRAG COEFFICIENT OF VARIOUS BOATTAILS AT MACH NUMBERS FROM 0.60 TO 1.47

By Douglas E. Harrington

Lewis Research Center
National Aeronautics and Space Administration
Cleveland, Ohio

ABSTRACT

The investigation was conducted in the Lewis 8- by 6-Foot Supersonic Wind Tunnel with two 15° conical boattails, a 20° conical boattail, and a 25° conical boattail. The 15° boattails had radii of curvature of 0 and 0.5 nacelle diameters at the juncture with the cylindrical nacelle. The base-to-nacelle-diameter ratio was 0.67 and the jet was simulated by a solid cylinder which had a diameter equal to the afterbody-base diameter. When compared with isolated boattail data, the presence of the rectangular wing reduced the axial-force coefficient over the entire range of variables tested. At subsonic and transonic speeds, the rectangular wing did not effectively simulate a complete airplane installation. However at supersonic speeds, agreement with complete airplane installation data was fairly good, particularly for the 15° boattail with a juncture curvature of 0 nacelle diameters. The effect of increasing boattail angle on pressure drag is influenced by the separation characteristics of these high-angle conical boattails.

SUMMARY

An investigation was conducted in the Lewis 8- by 6-Foot Supersonic Wind Tunnel with various afterbody models to determine the effect of a large rectangular wing on boattail pressure drag. These models consisted of two 15° conical boattails, a 20° conical boattail, and a 25° conical boattail. The 15° boattails had radii of curvature 0 and 0.5 nacelle diameters at the juncture with the cylindrical nacelle. The 20° and 25° conical boattails each had a radius of curvature of 0 at the afterbody juncture. Incidence angle between the nacelle and wing was also varied and had values of 0° and 4.5°. The conical forebody of the nacelle was closed, and the jet was simulated by a solid cylinder which had a diameter equal to the afterbody-base diameter. Data were obtained over a Mach number range from 0.60 to 1.47 with the wing positioned at 0° angle-of-attack.

When compared with isolated boattail data, the presence of the rectangular wing reduced boattail axial-force coefficient over the entire

range of variables tested. At subsonic and transonic speeds, the rectangular wing did not effectively simulate a complete airplane installation. However, at supersonic speeds, agreement with complete airplane installation data was fairly good, particularly for the 15° boattail ($r/d_m = 0$). For the 15° boattail ($r/d_m = 0.5$), boattail axial-force coefficients were lower in the presence of the rectangular wing than in the presence of a smaller, trapezoidal wing at Mach numbers from 0.6 to 0.85 and 0.95 to 1.00. At subsonic and transonic speeds, the incidence angle between the wing and nacelle had no effect on boattail axial-force coefficient. In general, at Mach numbers greater than 1.2, increasing the incidence angle from 0° to 4.5° decreased the axial-force coefficient approximately 5 to 10 percent. Increasing boattail angle from 15° to 25° generally increased boattail pressure drag at subsonic speeds but had little effect at supersonic speeds due to the separation characteristics of these high-angle conical boattails.

INTRODUCTION

As part of a program in airbreathing propulsion at the Lewis Research Center, various nozzle concepts, designed primarily for supersonic cruise application, are being studied at off-design conditions. Current airbreathing propulsion systems designed for supersonic flight operate over a wide range of nozzle pressure ratios. To maintain efficient operation at all flight speeds, variations in the nozzle exit area are required. At subsonic speeds, for example, the nozzle exit area will be smaller than that required at supersonic speeds. This reduction in exit area necessitates increased boattailing of the afterbody. The resultant drag can be a significant portion of the net thrust of the propulsion system, particularly at subsonic cruise, where the engine is at a reduced power setting.

Studies have been conducted to determine the drag characteristics of various isolated nacelle afterbodies, as reported in reference 1 to 3. However, these investigations do not account for installation effects. With an engine-nacelle installation typical of a supersonic cruise aircraft, the afterbody may be close to the lower surface of a large wing and may extend a short distance downstream of the wing trailing edge. Transonic wind tunnel model tests of this installation effect are difficult, however, because of blockage limitations and tunnel wall interference effects. One approach to the problem is to use small-scale complete-aircraft models as was done in reference 4. An alternate approach may be to utilize fairly large nacelle models but only a portion of the wing. This technique was used in reference 5 where a relatively small trapezoidal wing was utilized to simulate the aft portion of a wing for supersonic aircraft.

The results of that test indicate that the presence of the small simulated wing produced the same trend observed with the complete airframe model (ref. 4) in that it reduced the boattail axial-force coefficients over the entire range of variables tested. However, the magnitude of the effect was less than that of the complete model. Thus, it became of interest to study the effects of a larger simulated wing on the pressure drag of various afterbodies; particularly a wing that completely shields the nacelle forebody.

An investigation was conducted in the Lewis 8- by 6-Foot Supersonic Wind Tunnel with various afterbody models to determine the effects of a large rectangular wing on boattail pressure drag. All afterbodies were tested in the presence of a jet-boundary simulator. Incidence angle between the nacelle and wing was also varied and had values of 0° and 4.5°. Data were obtained over a Mach number range from 0.60 to 1.47 with the wing positioned at 0° angle-of-attack. The Reynolds number based on nacelle diameter ranged from 1.25×10^6 at Mach 0.60 to 1.65×10^6 at Mach 1.47.

APPARATUS AND PROCEDURE

The complete afterbody model with the simulated wing, as installed in the Lewis 8- by 6-Foot Supersonic Wind Tunnel, is shown in figure 1. The basic model was a sting-supported, 10.16-centimeter-diameter-cylindrical section with a 10° half-angle conical forebody. Figure 2 shows the details of the complete model installation. In order to avoid excessive aerodynamic loading, the wing was maintained at 0° angle-of-attack with free-stream flow. Incidence angle (i) between the nacelle centerline and wing was thus varied by increasing the angle-of-attack of the nacelle rather than the wing. Values of incidence angle included 0° and 4.5°. The rectangular wing had a maximum thickness-to-chord ratio of 14 percent. It was flat on the nacelle side and sharpened on the opposite side with leading-edge and trailing-edge wedge angles of 5° and 2.25°, respectively, leaving a flat center section. The nacelle forebody was aft of the wing-leading edge and completely sheltered by the wing. The boattails were downstream of the wing trailing edge at an extension ratio, l/d_m, of 0.97. The nozzle extension ratio was the same for all boattails and is defined as the distance from the wing-trailing edge to the nozzle-exit plane divided by the maximum model diameter. The smaller trapezoidal wing that was used in reference 5 is also shown and is represented by the dashed lines. In that test the cylindrical nacelle was approximately 1.5 times as long as the nacelle in the present test. In addition, the nacelle forebody extended forward of the leading edge of the trapezoidal wing. However, the location of the boattail relative to the wing-trailing edge was similar to that of the present investigation. Each of the boattails was tested with a jet-boundary simulator extending aft from the

afterbody base. The purpose of the simulator was to approximate the local flow field that would exist if a fully-expanded jet were present with an exit-to-local-static-pressure ratio of 1.0.

The afterbody geometries which were investigated are shown in figure 3. These included a cylindrical afterbody with boundary-layer rakes, two 15° conical boattails, a 20° conical boattail, and a 25° conical boattail. The two boundary-layer rakes on the cylindrical afterbody were located 6.48 centimeters aft of the nacelle-afterbody interface. This position coincides with the location of the corner of the sharp 15° boattail ($r/d_m \doteq 0$). The two 15° conical boattails had radii of curvature of 0 and 0.5 nacelle diameters at the juncture with the cylindrical nacelle. The 20° and 25° conical boattails each had a radius of curvature of 0 at the afterbody juncture. The base-to-nacelle-diameter ratio was maintained constant at a value of 0.67 for all of the boattail configurations.

Details of the boundary-layer rakes are shown in figure 4. The bottom rake (180°) measured a boundary layer that had been modified by the wing while the top rake (0°) was relatively free of installation effects. The total pressures from the rakes were used with local static pressures to compute values of V/V_0 using the Rayleigh-pitot equation.

Typical afterbody instrumentation is presented in figure 5. The boattail static pressure orifices are shown for the 15°, $r/d_m = 0$ configuration but these are representative of all of the boattailed afterbodies tested. The location of boattail static pressure instrumentation for all configurations tested is listed in table I. The axial projection of the boattail was divided into ten equal annular areas. Three rows of ten orifices each were located at 0°, 180°, and 270° (looking upstream). It was assumed that the local flow field would be symmetrical about the vertical centerline, so pressures were located on only one side of the boattail. By instrumenting the boattail in this manner, an area-weighted average of pressure coefficients can be computed. This average pressure coefficient is then used to compute the axial-force coefficient. The boattail axial-force coefficient computed in this manner does not include the afterbody-base drag or afterbody-skin-friction drag but pertains only to pressure forces acting on the boattail surface. Nacelle static-pressure instrumentation and location is shown in figure 6. In addition, static-pressure instrumentation is also shown for the cylindrical afterbody configuration.

RESULTS AND DISCUSSION

The effect of the large rectangular wing installation on boattail axial-force coefficient is presented in figure 7 for the three boattails with $r/d_m = 0$. These data are presented for an incidence angle of 4.5°. When compared with isolated nacelle data, the presence of the rectangular

wing reduced boattail axial-force coefficient over the entire range of variables tested. For example, for the 15° boattail, fig. 7(a), at a free-stream Mach number of 0.90, boattail axial-force coefficient was reduced by 48 percent due to the presence of the simulated wing. The effect of a complete airplane installation on boattail axial-force coefficient is shown using unpublished Lewis data in which a 1/20 scale F-106 airplane model was used. The nacelles used with the 1/20 scale F-106 model were geometrically similar to those used in the present test. The location of the boattails with respect to the trailing edge of the wing was also duplicated. The nacelle installation on the F-106 model is presented in detail in reference 4. At subsonic speeds, boattail axial-force coefficient was lower in the presence of the complete airplane installation than in the presence of the rectangular wing. In other words, the rectangular wing did not effectively simulate a complete airplane installation at these lower speeds. In addition, due to the small scale of the F-106 model relative to the rectangular wing model, the ratio of boundary-layer thickness to model diameter was probably larger for the airplane model than for the simulated wing model; and, in general, the thicker the boundary layer, the lower the boattail-drag coefficient. At supersonic speeds, agreement with complete airplane installation data was fairly good, particularly for the 15° boattail ($r/d_m = 0$).

For all of the configurations in the presence of the rectangular wing, a dip occurred in the drag coefficient curves at $M_0 = 1.02$. This phenomena resulted from the higher pressures caused by a terminal shock wave on the boattail. The flow field near the front of an ogive-cylinder creates a terminal shock which moves aft rapidly with increasing flight velocity and disappears downstream at speeds near Mach 1. Thus, the resultant boattail pressure drag can be influenced by the presence of a terminal shock as it passes over the boattail. This phenomena is discussed more thoroughly in reference 6. No dip was apparent for the isolated boattail due to the limited amount of data at transonic speeds.

A comparison of the rectangular and trapezoidal wing data (ref. 5) is presented in figure 8 for the 15° boattail ($r/d_m = 0.5$) and a wing incidence angle of 0°. Isolated nacelle data are also presented. The trapezoidal wing data were interpolated from reference 5 for an extension ratio (l/d_m) equal to 0.97. When compared with isolated boattail data, the presence of the rectangular wing reduced boattail axial-force coefficient over a range of subsonic Mach numbers from 0.60 to 1.00. For example, at a free-stream Mach number of 0.90, boattail axial-force coefficient was reduced by 74 percent due to the presence of the rectangular wing. When compared with the data for the smaller trapezoidal wing, boattail axial-force coefficients were generally lower in the presence of the larger rectangular wing at Mach numbers from 0.60 to 0.85 and from 0.95 to 1.00.

Figure 9 shows the effect of wing incidence angle on boattail axial-force coefficient for the 15° ($r/d_m = 0.5$) boattail. Compared with isolated data, the presence of the rectangular wing, either at 0° or 4.5° incidence, reduced the boattail axial-force coefficient. At subsonic and transonic speeds, the incidence angle had little effect on boattail axial-force coefficient. In general, at Mach numbers greater than 1.2, increasing the incidence angle from 0° to 4.5° decreased the axial-force coefficient approximately 5 to 10 percent.

The effect of boattail angle on boattail axial-force coefficient is presented in figure 10 for the $r/d_m = 0$ boattails. Data are shown for both the isolated case, fig. 10(a), and with the wing at 4.5° incidence, fig. 10(b). Subsonically for the isolated boattails, increasing boattail angle generally increased the axial-force coefficient At supersonic speeds, however, the axial-force coefficients for the 25° boattail were lower than the coefficients for both the 15° and 20° boattails. As will be discussed later, these results are influenced by the separation characteristics of these high-angle conical boattails. In the presence of the wing ($i = 4.5°$) at subsonic speeds, increasing boattail angle again generally increased the axial-force coefficient. At transonic and supersonic speeds, the influence of boattail angle on boattail drag was smaller and again influenced by separation characteristics.

Figure 11 shows the effect of boattail juncture radius of curvature on boattail axial-force coefficient for the 15° boattails both isolated and with the wing at 4.5° incidence. Increasing the boattail juncture radius of curvature decreased boattail axial-force coefficient both isolated and under the influence of the rectangular wing. The effect of the radius of curvature on boattail drag is discussed in more detail in reference 2.

Pressure distributions along the side of the nacelle surface (90° from the vertical centerline) are presented in figure 12. Data are shown for the cylindrical afterbody. In general, the presence of the rectangular wing reduced the local pressure in the region under the wing and had no effect on pressure levels on the afterbody surface aft of the wing-trailing edge compared to an isolated nacelle. Figure 13 presents pressure distributions along the vertical centerline of the nacelle. Data are again shown for the cylindrical afterbody. The presence of the rectangular wing reduced the local pressure in the region under the wing compared to an isolated nacelle at all test Mach numbers. In addition, the wing also appeared to delay the recompression from the cone shoulder. Subsonically, the presence of the wing had no effect on the pressure levels on the afterbody surface aft of the wing-trailing edge compared to an isolated nacelle. In general, at supersonic speeds pressure levels on the afterbody surface were decreased due to the influence of the wing.

Boattail pressure distributions are presented in figures 14-17 for all four boattail configurations tested. Data are shown for orifices located at 0°, 180°, and 270° circumferentially. In addition, isolated nacelle data are presented for comparison. Boattail pressure distributions for the 15° boattails are shown in figures 14 and 15. Generally speaking, the presence of the rectangular wing increased the pressures on the 15° boattails when compared with the isolated case. With the wing incidence angle at 0°, fig. 15, the flow initially expanded to higher pressures at 180° circumferentially than at either 0° or 270°. However, at the trailing edge of the boattail, the pressures were lower at 180° than at 0° and 270°. With the wing incidence angle at 4.5° the highest pressures occurred at 0° circumferentially. No flow separation was noted for the 15° boattails. Figure 16 presents boattail pressure distributions for the 20° conical boattail. In general, the pressures at 0° and 270° circumferentially were higher than for the isolated case. The pressures at 180° circumferentially were generally lower than for the isolated case at the shoulder of the boattail. However, the flow at 180° did compress to pressures higher than for the isolated case at the trailing edge of the boattail. Flow separation occurred for the isolated 20° boattail at Mach numbers greater than 0.90.

Flow separation apparently was asymmetric over the 20° conical boattail in the presence of the wing. Separation was observed at 0° and 270° circumferentially. However, at 180° the flow did not appear to be separated. Figure 17 presents boattail pressure distributions for the 25° conical boattail. As before, the presence of the wing increased boattail pressures when compared with the isolated nacelle case. Flow separation occurred for the isolated 25° boattail at Mach numbers between 0.6 and 1.27. Flow separation appeared to be asymmetric in the presence of the wing and was observed at all Mach numbers. No separation occurred at 180° for Mach numbers of .60, .70, and 1.20 to 1.47. However, at the remaining test Mach numbers, the flow at 180° also appeared to be separated.

The effect of the rectangular wing on afterbody boundary-layer characteristics is presented in figure 18. The boundary layer on the top of the model (away from the wing) at various Mach numbers is shown in figure 18(a). The presence of the wing generally reduced the local velocity compared to V_0 at subsonic speeds and increased it at supersonic speeds. The major effect was an increase in boundary-layer thickness for an incidence angle of 4.5°. For this condition, the boundary layer is being measured on the leeward side of cone-cylinder body at a 4.5° angle-of-attack. The increased thickness results from cross flow at the end of the nacelle.

The effect of the wing on the boundary-layer characteristics on the bottom (or wing side) of the model is presented in figure 18(b). As expected, the local velocities are influenced more by the presence of the wing at this location since this rake is in the wake of the wing. In general, the local velocities were lower than free-stream

values at all Mach numbers, particularly for an incidence angle of 4.5°. This is expected since the rake is on the windward side of a nacelle at 4.5° angle-of-attack to the free stream. For this same reason, the boundary layer thins out when the incidence angle increased from 0 to 4.5°.

The variations in boundary-layer momentum thickness over a range of Mach number are summarized in figure 19 at the top and bottom of the nacelle for incidence angles of 0 and 4.5°. As discussed previously there is a general increase in momentum thickness on the leeward side (top) of the model at an incidence angle of 4.5°. The addition of the wing increases the momentum thickness on the bottom of the model, as expected, for an incidence angle of zero. The momentum thickness decreases as the incidence angle increases to 4.5° since the measurement is made on the windward side of the nacelle.

SUMMARY OF RESULTS

An investigation was conducted in the Lewis 8- by 6-Foot Supersonic Wind Tunnel with various afterbody models to determine the effect of a large rectangular wing on boattail pressure drag. These models consisted of two 15° conical boattails, a 20° conical boattail, and a 25° conical boattail. The 15° boattails had radii of curvature of 0 and 0.5 nacelle diameters at the juncture with the cylindrical nacelle. The 20° and 25° conical boattails each had a radius of curvature of 0 nacelle diameters at the afterbody juncture. Incidence angle between the nacelle and wing was also varied and had values of 0° and 4.5°. The conical forebody of the nacelle was closed, and the jet was simulated by a solid cylinder which had a diameter equal to the afterbody-base diameter. Data were obtained over a Mach number range from 0.60 to 1.47 with the wing positioned at 0° angle-of-attack. The following results were obtained:

1. When compared with isolated boattail data, the presence of the rectangular wing reduced boattail axial-force coefficient over the entire range of variables tested.

2. At subsonic and transonic speeds, the rectangular wing did not effectively simulate a complete airplane installation. However, at supersonic speeds agreement with complete airplane installation data was fairly good, particularly for the 15° conical boattail.

3. For the 15° boattail ($r/d_m = 0.5$) boattail axial-force coefficients were generally lower in the presence of the rectangular wing than in the presence of a smaller, trapezoidal wing at Mach numbers up to 1.00.

4. At subsonic and transonic speeds, the incidence angle between the wing and nacelle had little effect on boattail axial-force coefficient. In general, at Mach numbers greater than 1.20, increasing the incidence angle from 0° to 4.5° decreased the axial-force coefficient approximately 5 to 10 percent.

5. Increasing boattail angle from 15° to 25° generally increased boattail pressure drag at subsonic speeds. The effect of boattail angle at supersonic speeds was smaller due to the separation characteristics of these high-angle conical boattails.

6. Increasing the boattail juncture radius of curvature decreased boattail axial-force coefficient for the 15° boattails both isolated and under the influence of the rectangular wing.

SYMBOLS

A	cross-sectional area
c	chord of wing
C_a	boattail axial-force coefficient, (boattail axial force)/$q_0 A_M$
C_p	pressure coefficient, $(p-p_0)/q_0$
d	diameter
i	incidence angle between the nacelle centerline and the wing
l	length from afterbody base to wing-trailing edge
M	Mach number
P	total pressure
p	static pressure
q	dynamic pressure
r	boattail-juncture radius of curvature
t	thickness of wing
V	velocity
x	axial distance aft of nacelle-afterbody interface

x_m axial distance aft of forebody shoulder

y radial distance from model surface

β boattail trailing-edge angle

δ^{**} boundary-layer momentum thickness

Subscripts

a axial

e nozzle-exit conditions

l local

m model nacelle

0 free-stream conditions

β boattail surface

REFERENCES

1. Silhan, Frank V.; and Cubbage, James M., Jr.: Drag of Conical and Circular-Arc Boattail Afterbodies at Mach Numbers From 0.6 to 1.3. NACA RM L56K22, 1957.

2. Shrewsbury, George D.: Effect of Boattail Juncture Shape on the Pressure Drag Coefficients of Isolated Afterbodies. NASA TM X-1517, 1968.

3. Harrington, Douglas E.: Jet Effects on Boattail Pressure Drag of Isolated Ejector Nozzles at Mach Numbers From 0.60 to 1.47. NASA TM X-1785, 1969.

4. Blaha, Bernard J.; and Mikkelson, Daniel C.: Wind Tunnel Investigation of Airframe Installation Effects on Underwing Engine Nacelles at Mach Numbers From 0.56 to 1.46. NASA TM X-1683, 1968.

5. Shrewsbury, George D.: Effect of a Simulated Wing on the Pressure Drag Coefficients of Various 15° Boattails at Mach Numbers From 0.56 to 1.00. NASA TM X-1662, 1968.

6. Mitchell, Glenn A.: Effect of Model Forebody Shape on Perforated Tunnel Wall Interference. NASA TM X-1656, 1968.

Table I - Afterbody Static-Pressure Orifice Locations [a]

Orifice Number	x/d_m			
	15° Boattail $r/d_m=0$	15° Boattail $r/d_m=0.5$	20° Boattail $r/d_m=0$	25° Boattail $r/d_m=0$
1	0.667	0.656	0.819	0.915
2	0.715	0.715	0.859	0.945
3	0.772	0.772	0.899	0.976
4	0.830	0.830	0.940	1.009
5	0.885	0.885	0.983	1.042
6	0.945	0.945	1.028	1.077
7	1.010	1.010	1.074	1.114
8	1.070	1.070	1.122	1.151
9	1.140	1.140	1.173	1.191
10	1.212	1.212	1.226	1.232

[a] See Figure 7

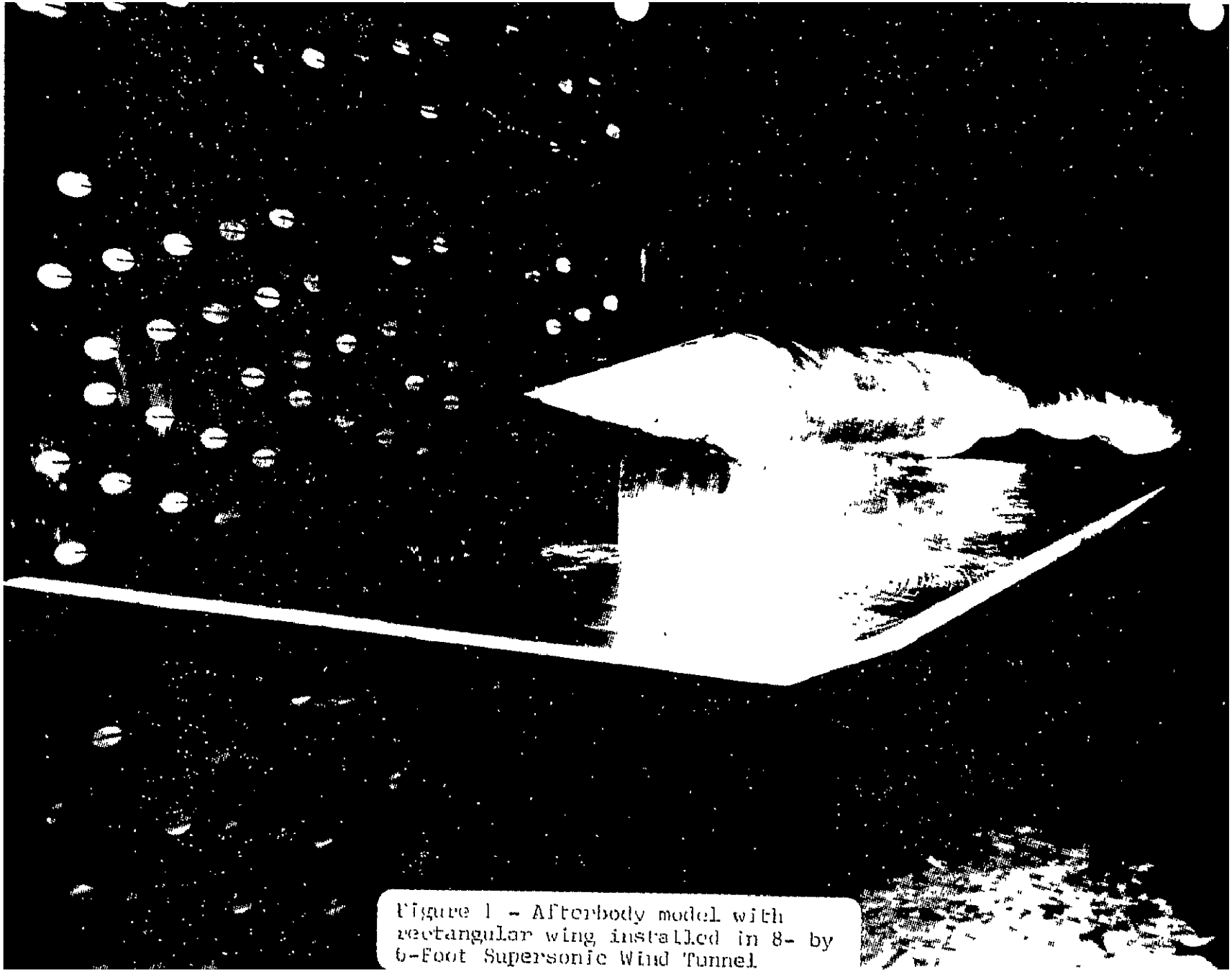

Figure 1 - Afterbody model with rectangular wing installed in 8- by 6-Foot Supersonic Wind Tunnel

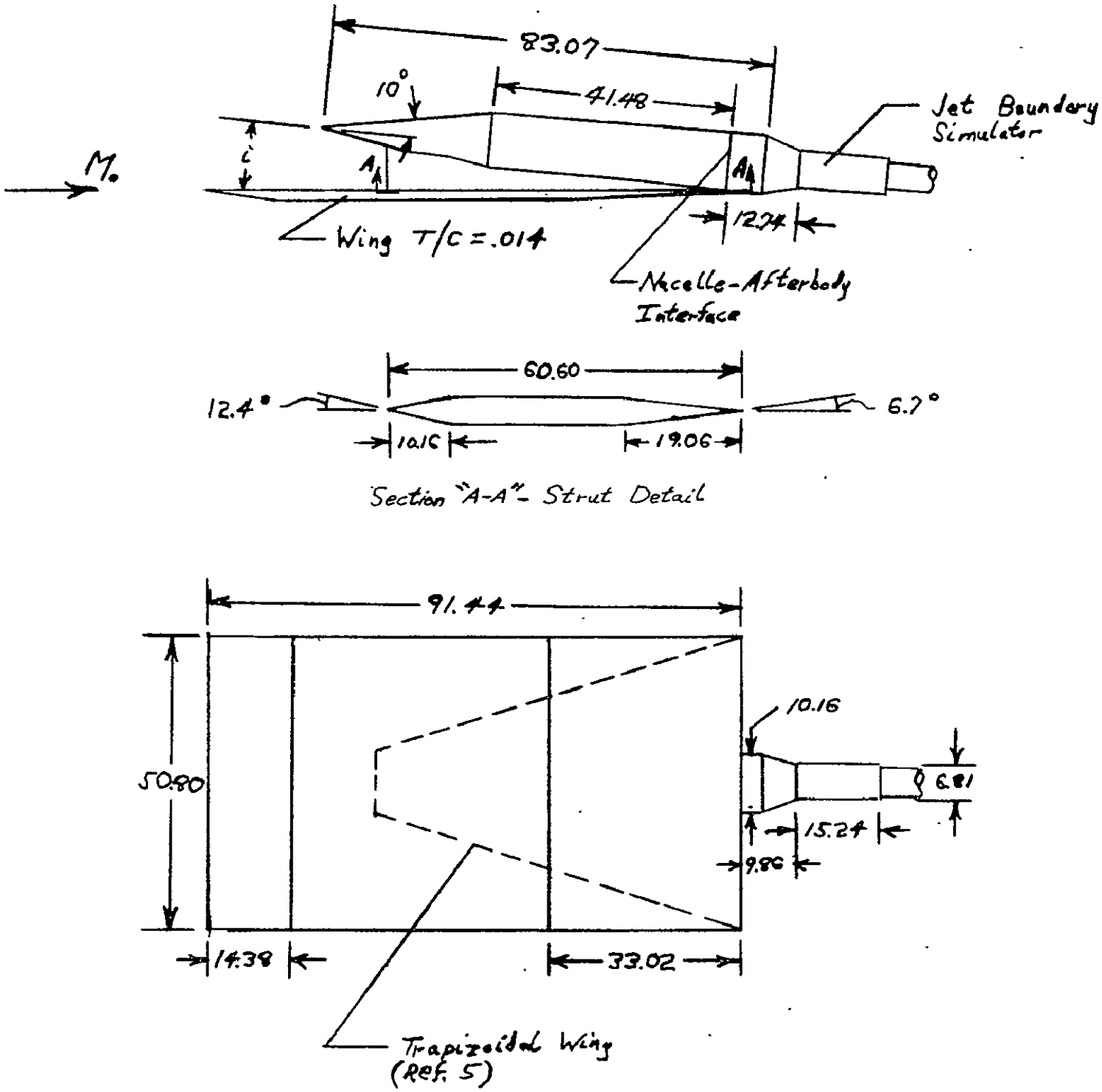

Figure 2 - Schematic diagram of nacelle and simulated wings

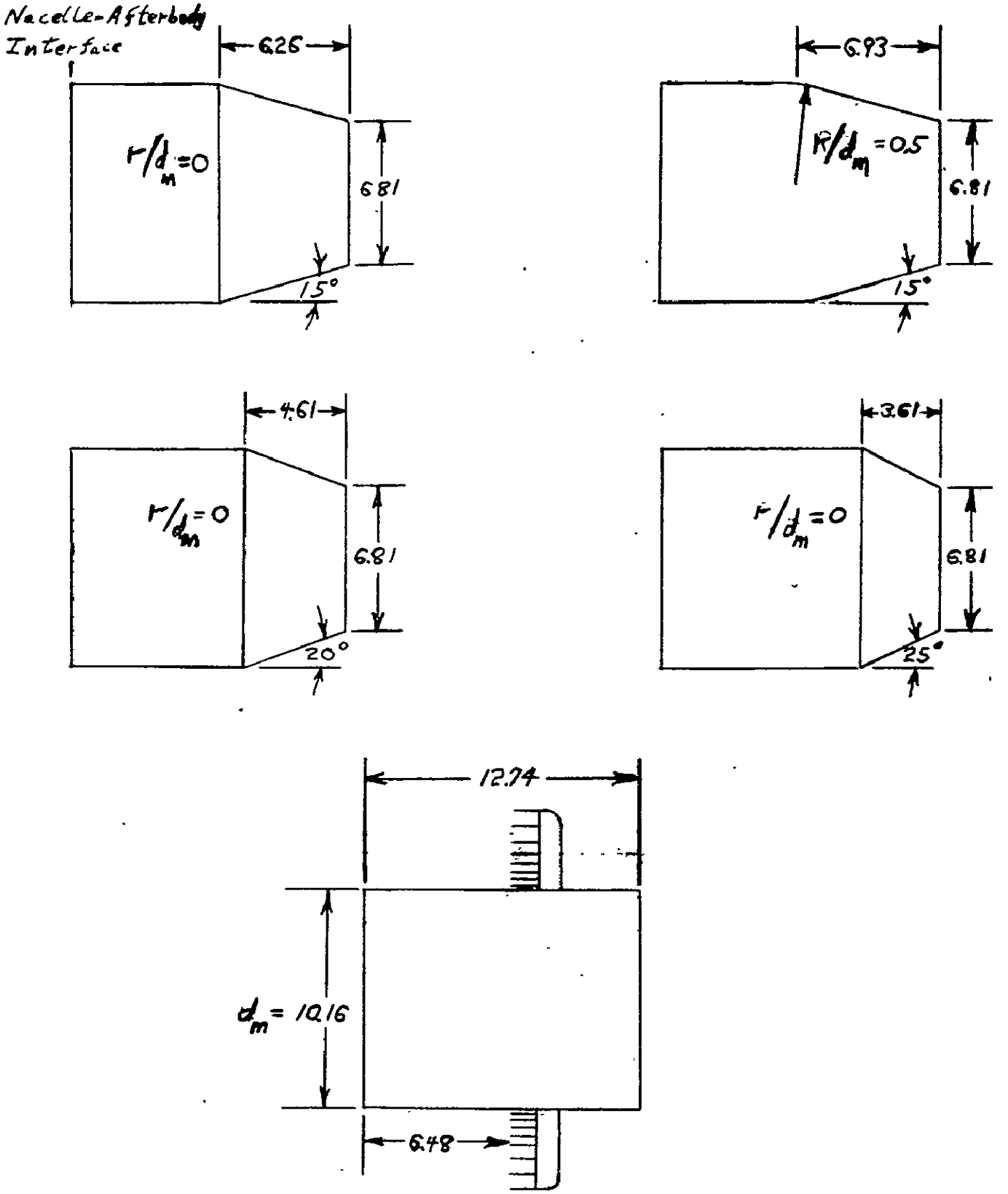

Figure 3 - Afterbody geometry details (all dimensions in centimeters)

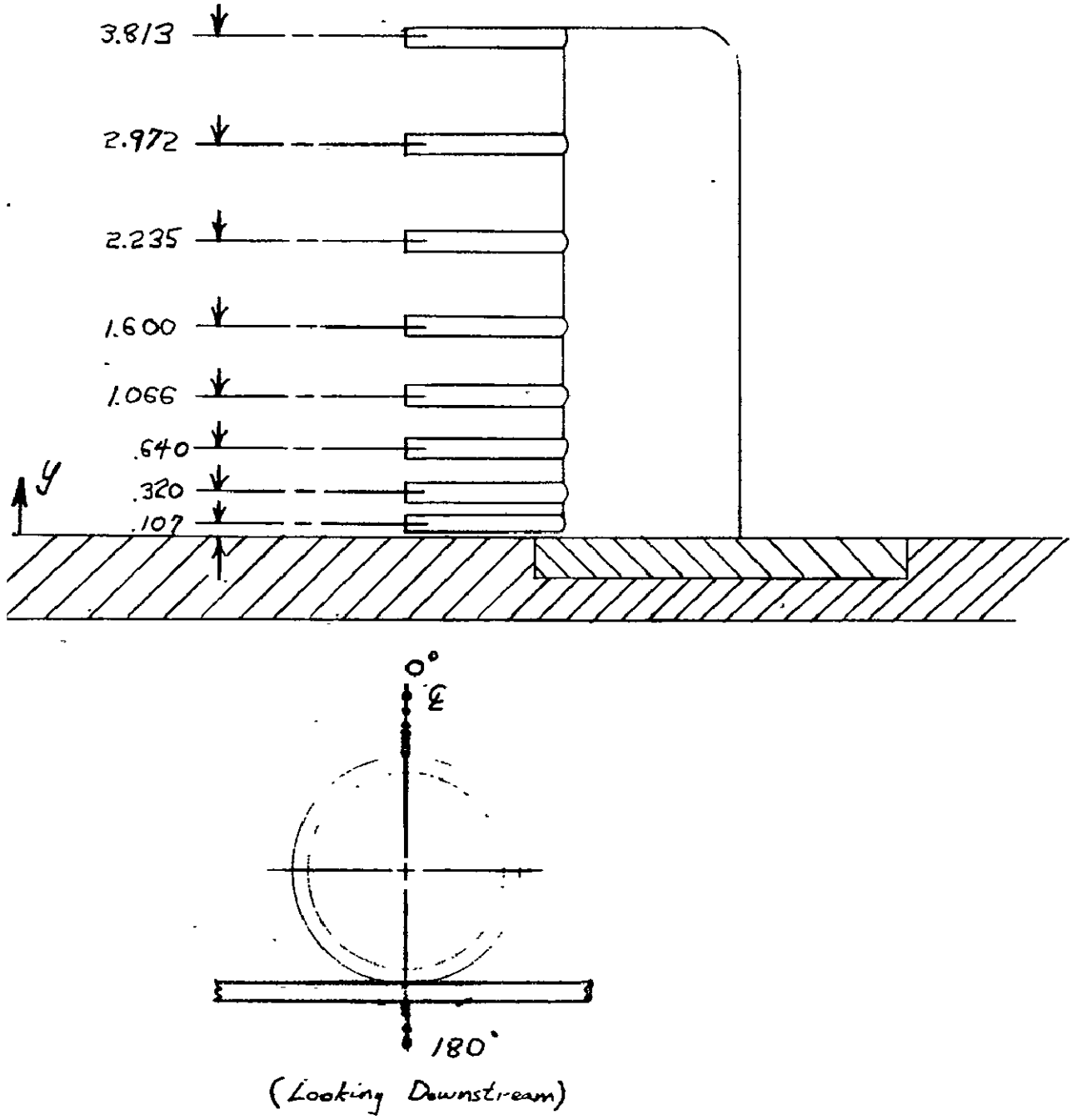

Figure 4 - Boundary layer rake details (all dimensions in centimeters)

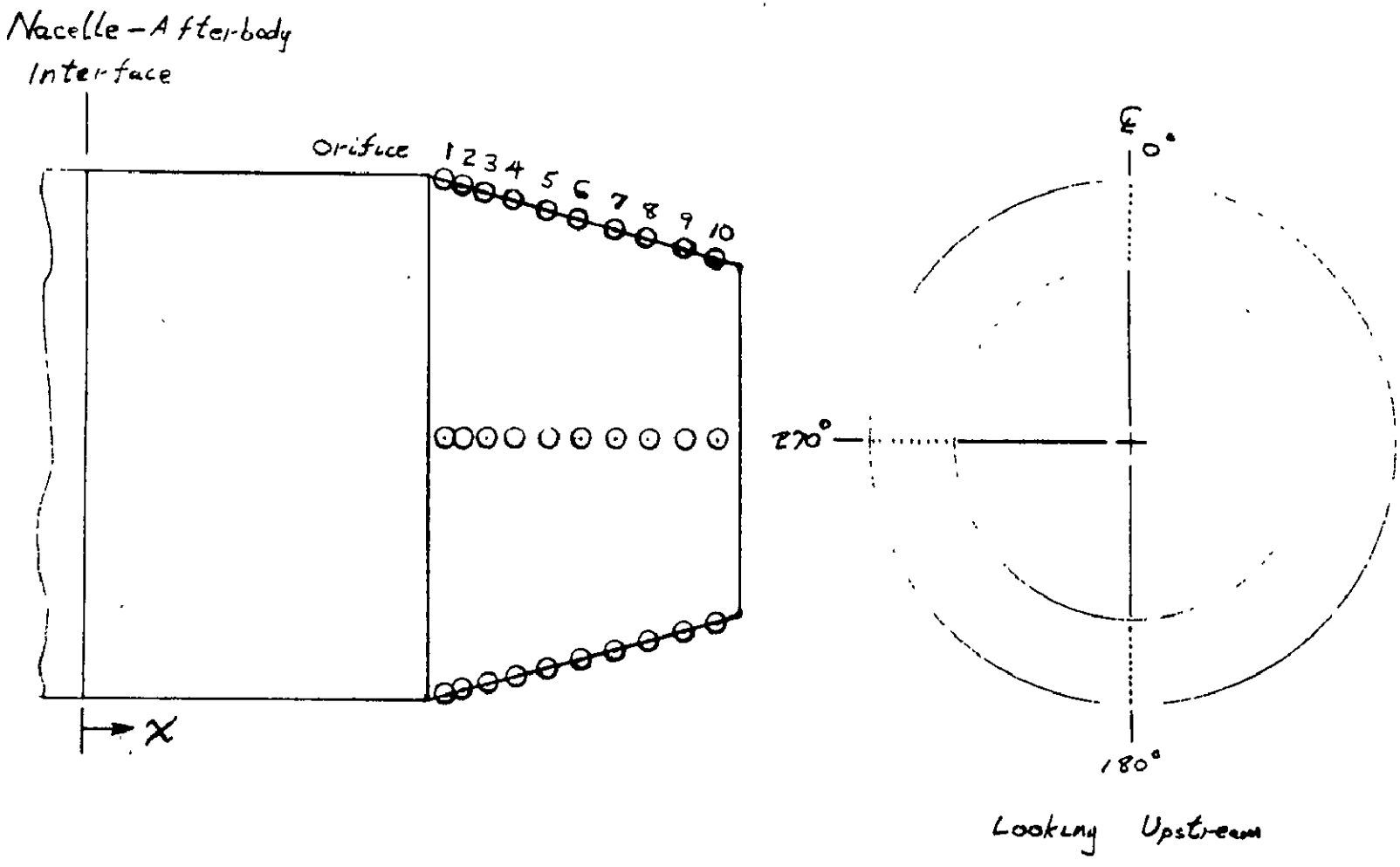

Figure 5 - Typical afterbody instrumentation details (see Table I for orifice coordinates)

Orifice Number	x/d_m	
	0°	270°
1	0.32	0.32
2	0.82	0.82
3	1.32	1.32
4	1.82	1.82
5	2.32	2.32
6	2.82	2.82
7	3.32	3.32
8	3.82	3.82
9	4.21	4.21
10	4.45	4.70
11	–	5.21

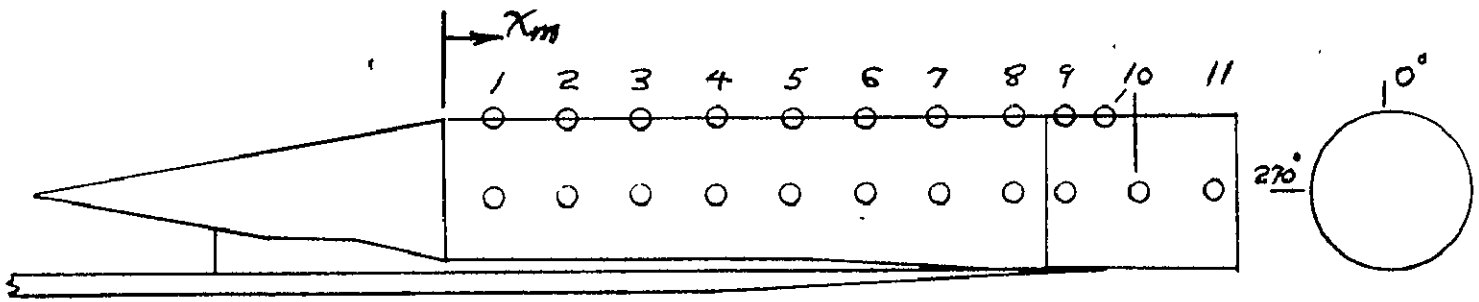

Figure 6 - Nacelle static-pressure orifice locations

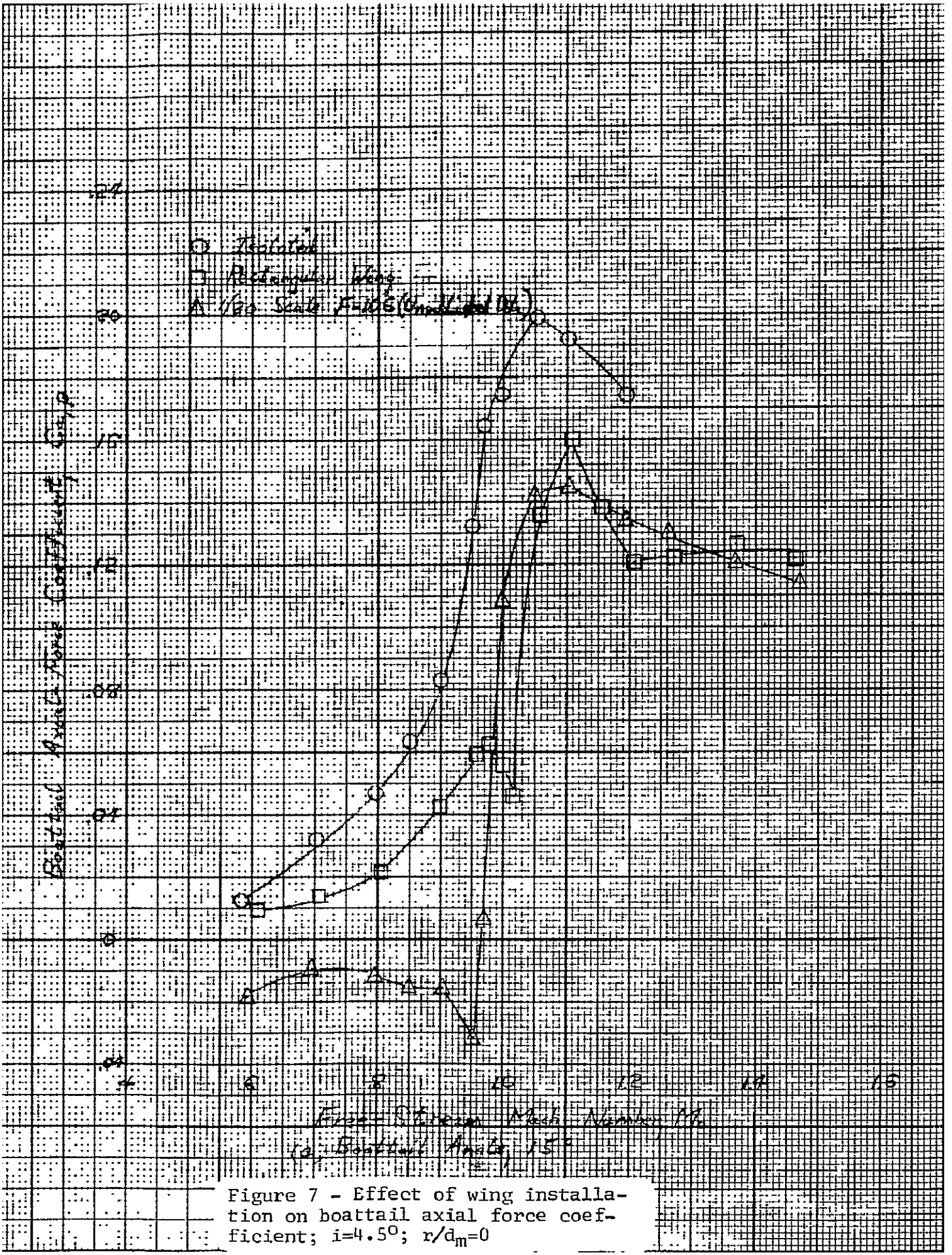

Figure 7 - Effect of wing installation on boattail axial force coefficient; $i=4.5^{o}$; $r/d_m=0$

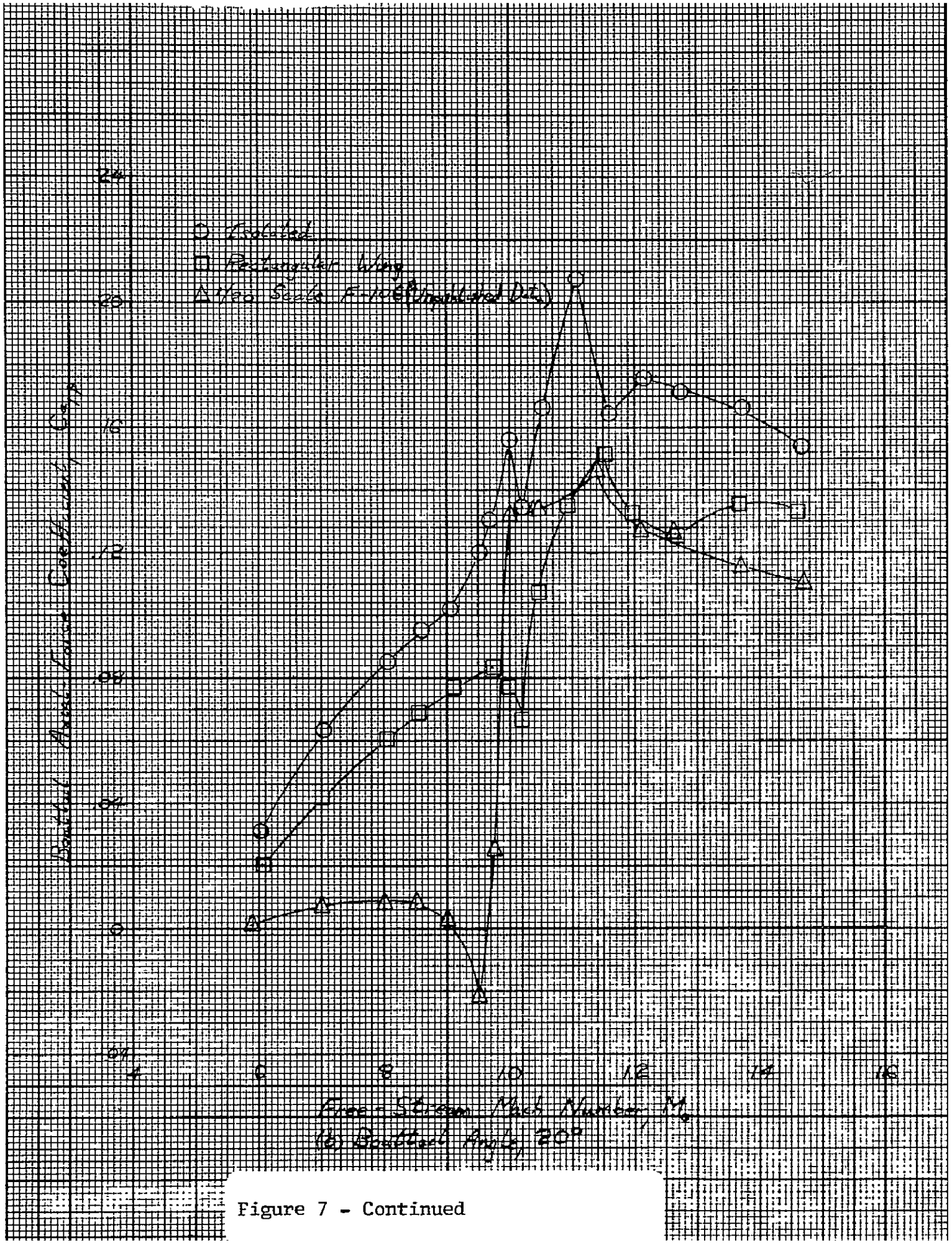

Figure 7 - Continued

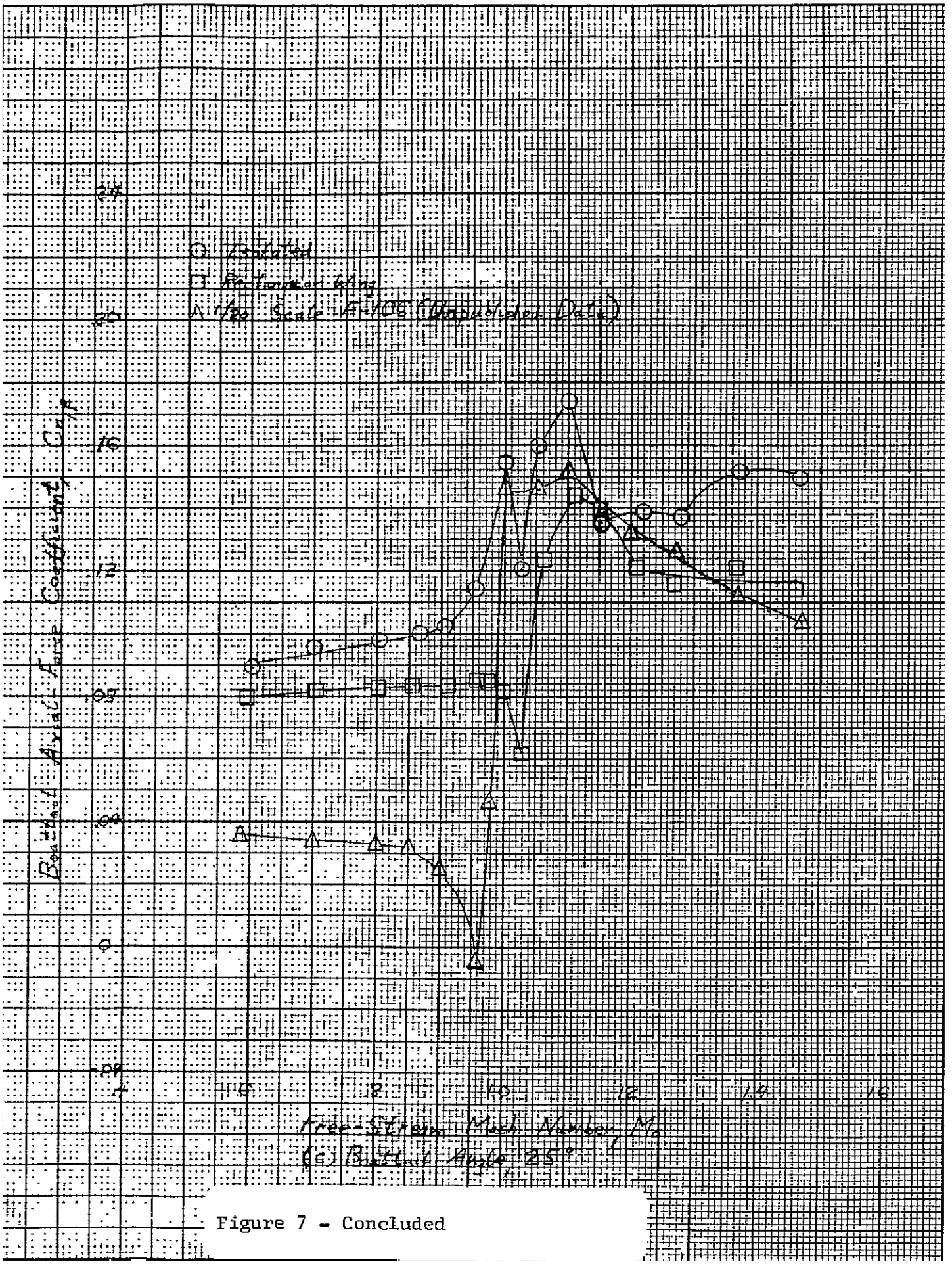

Figure 7 - Concluded

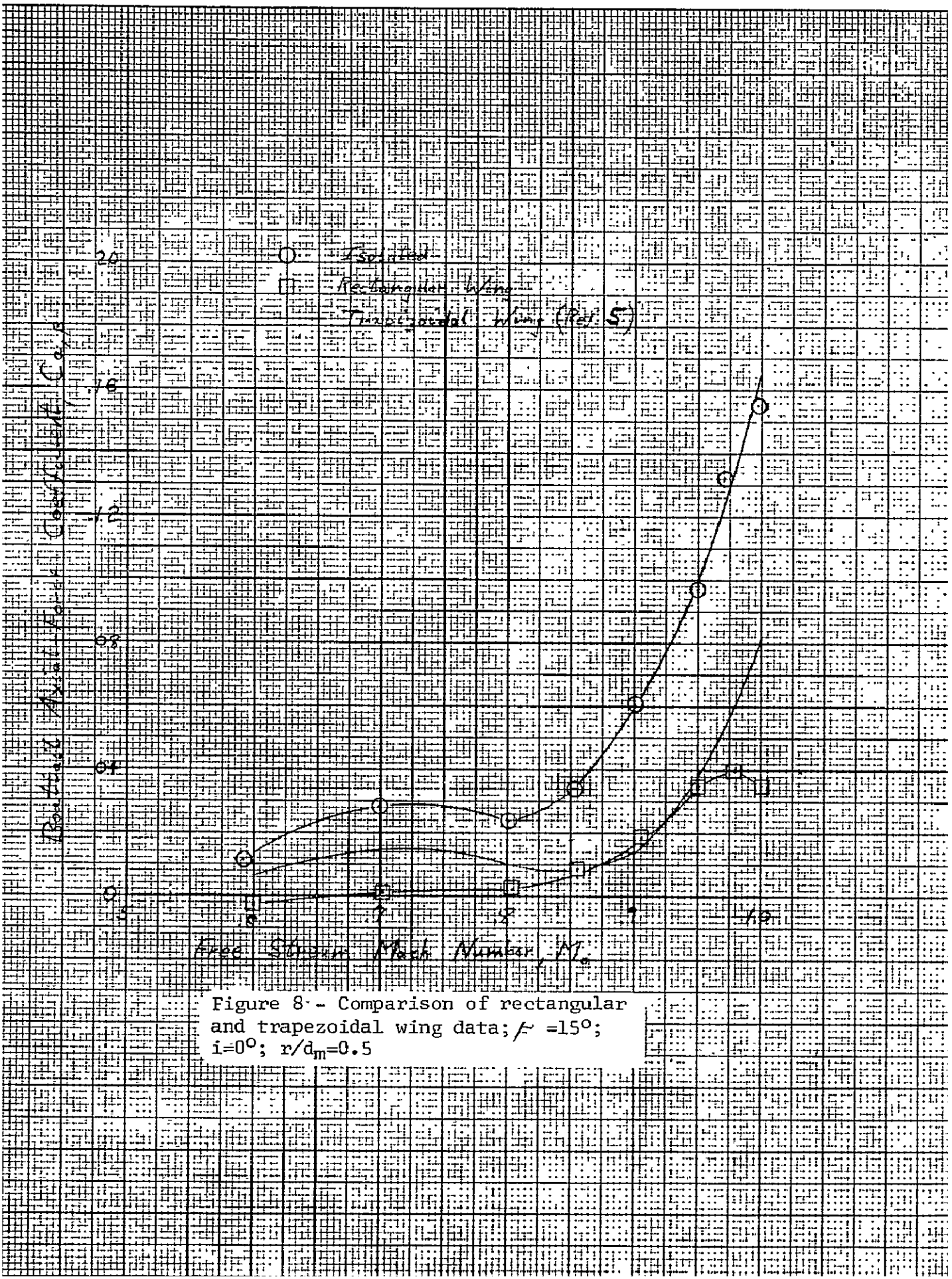

Figure 8 - Comparison of rectangular and trapezoidal wing data; Λ =15°; i=0°; r/d_m=0.5

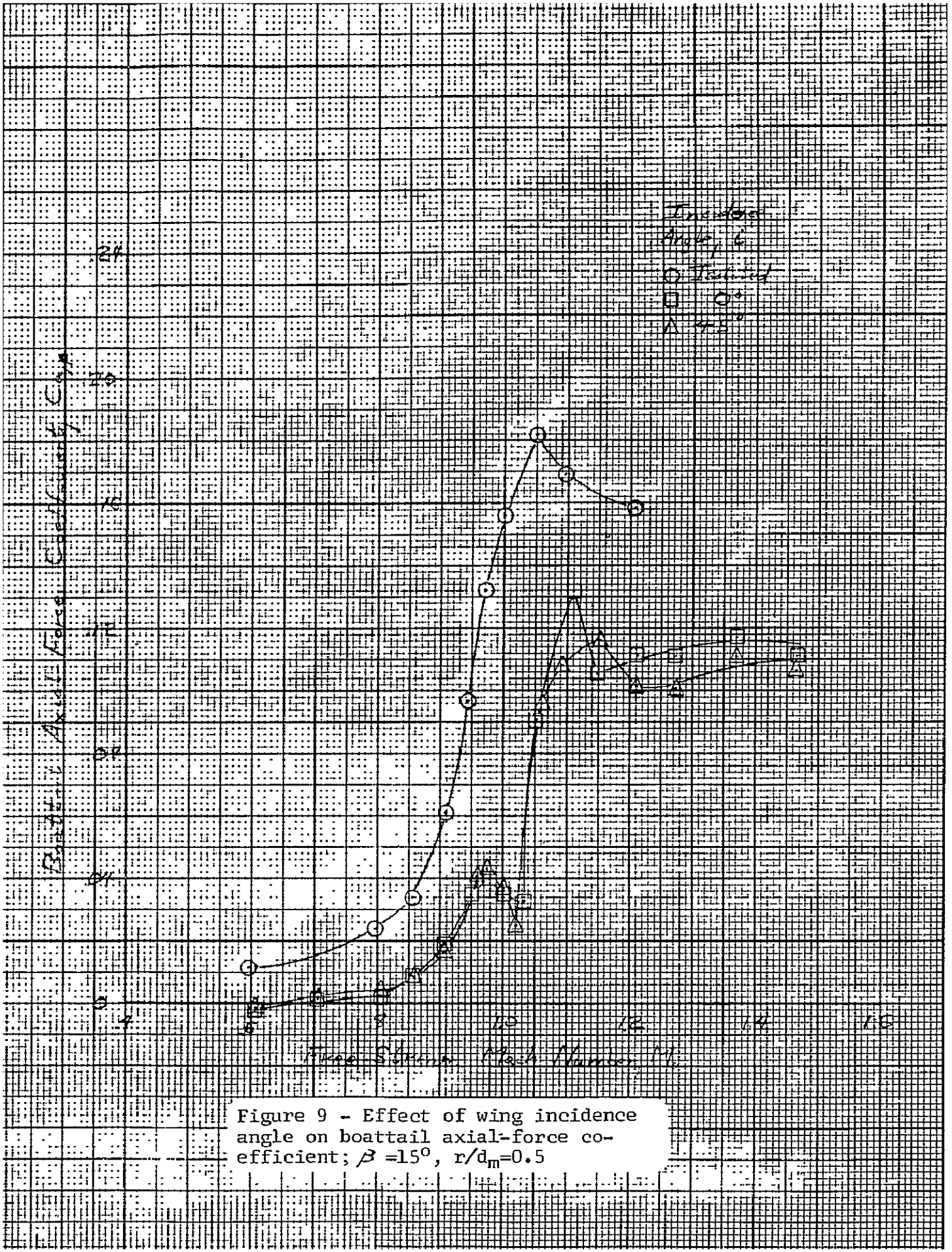

Figure 9 - Effect of wing incidence angle on boattail axial-force coefficient; $\beta = 15^{o}$, $r/d_m = 0.5$

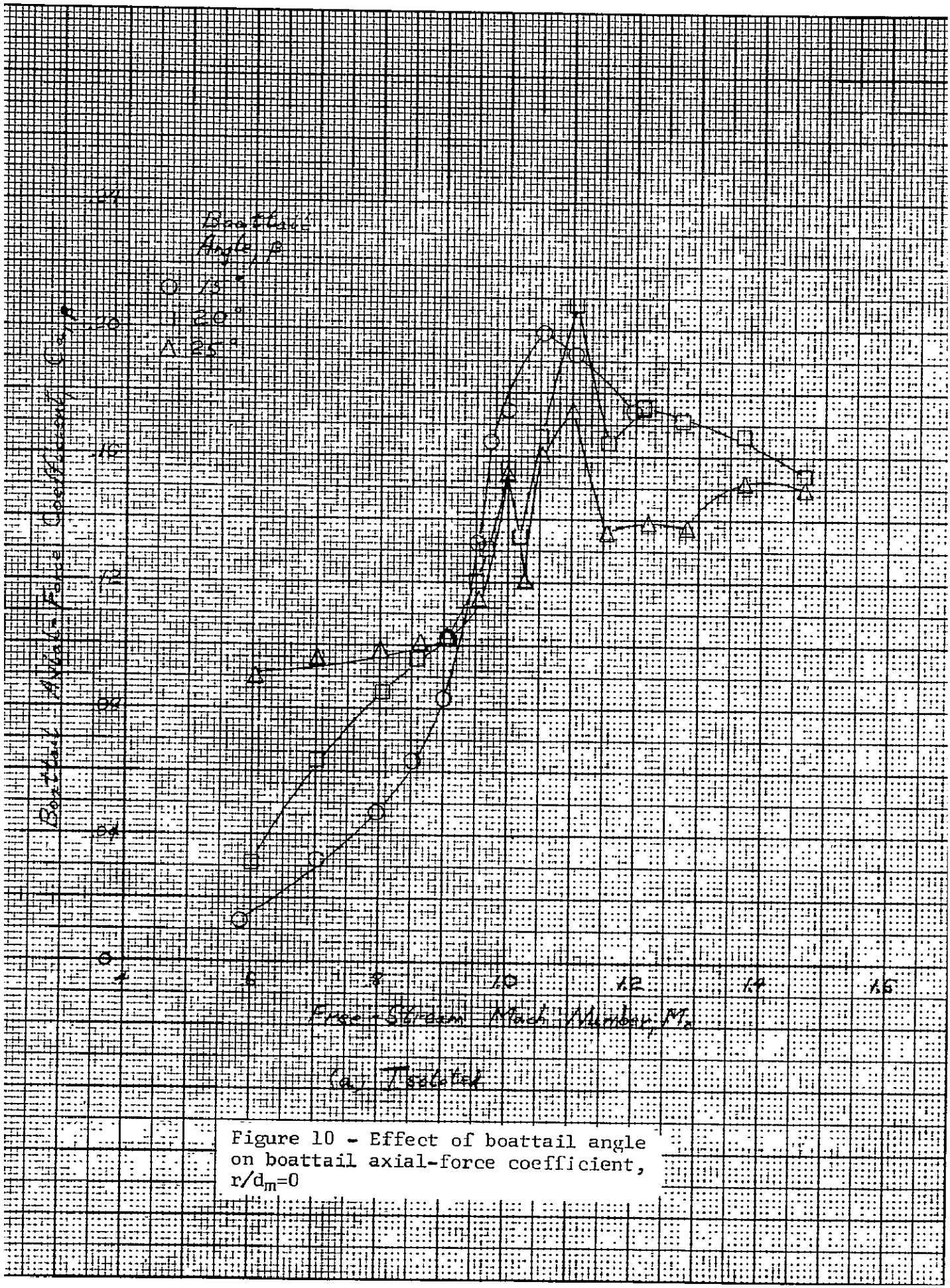

Figure 10 - Effect of boattail angle on boattail axial-force coefficient, $r/d_m=0$

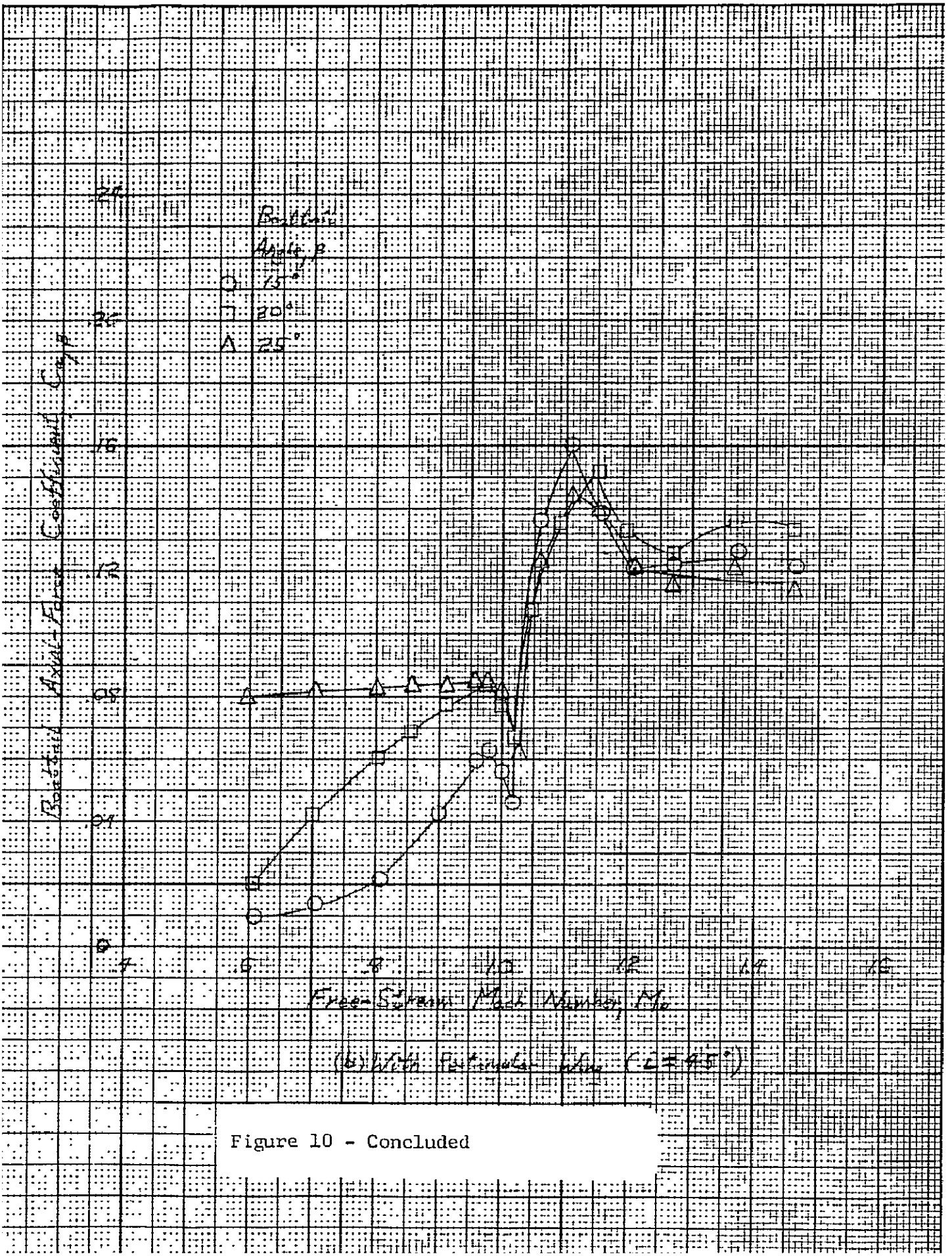

Figure 10 - Concluded

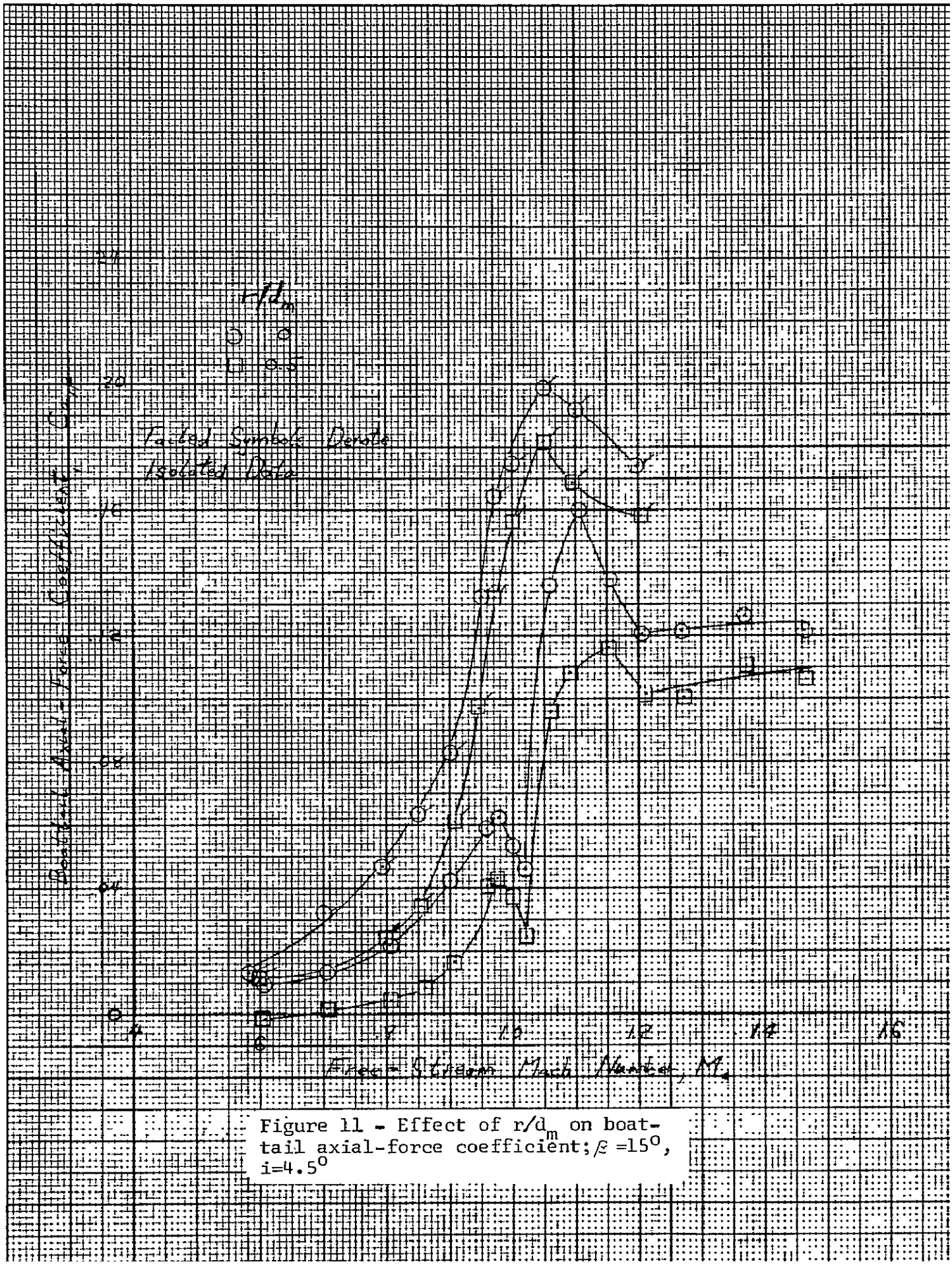

Figure 11 - Effect of r/d_m on boat-tail axial-force coefficient; $\beta = 15^\circ$, $i = 4.5^\circ$

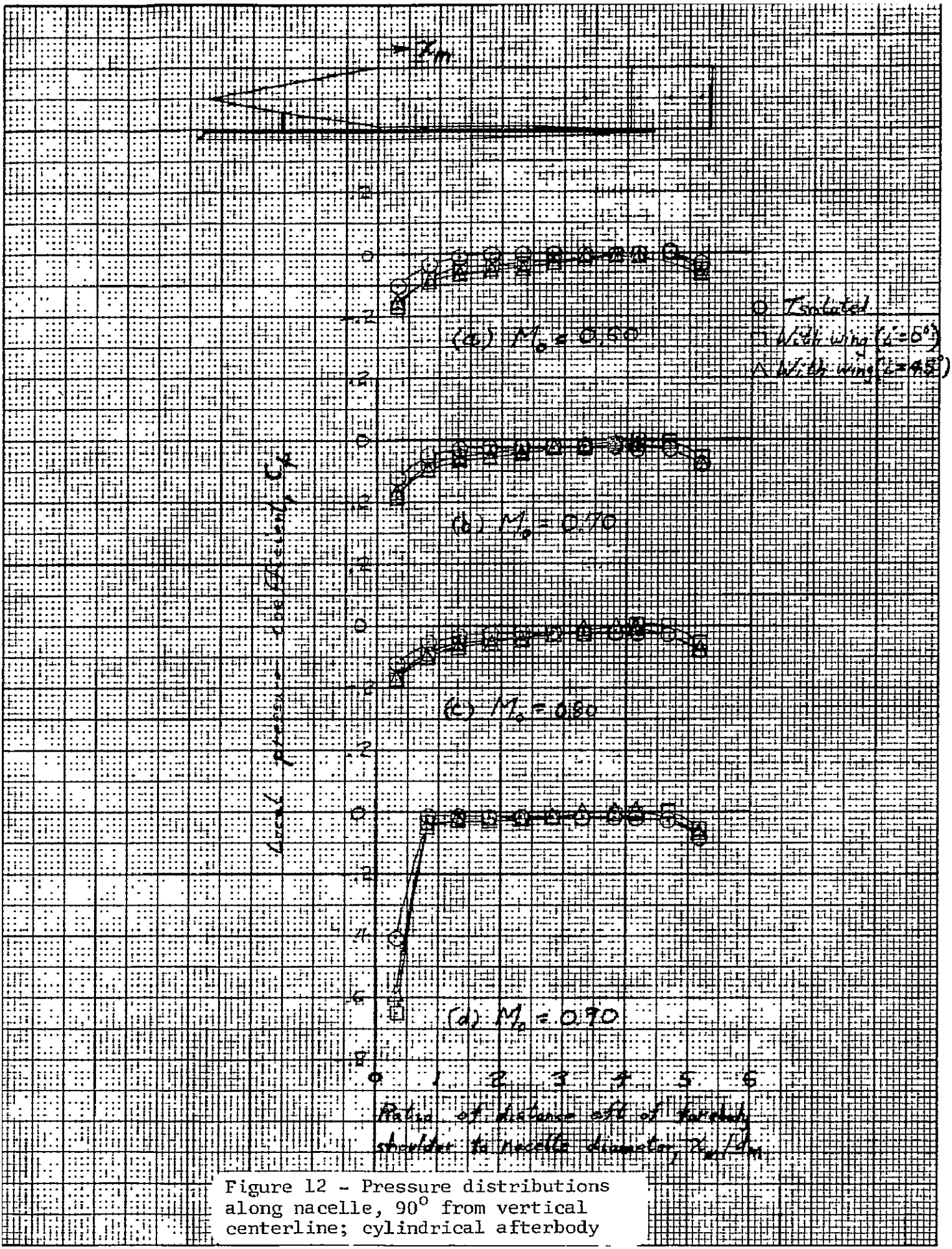

Figure 12 - Pressure distributions along nacelle, 90° from vertical centerline; cylindrical afterbody

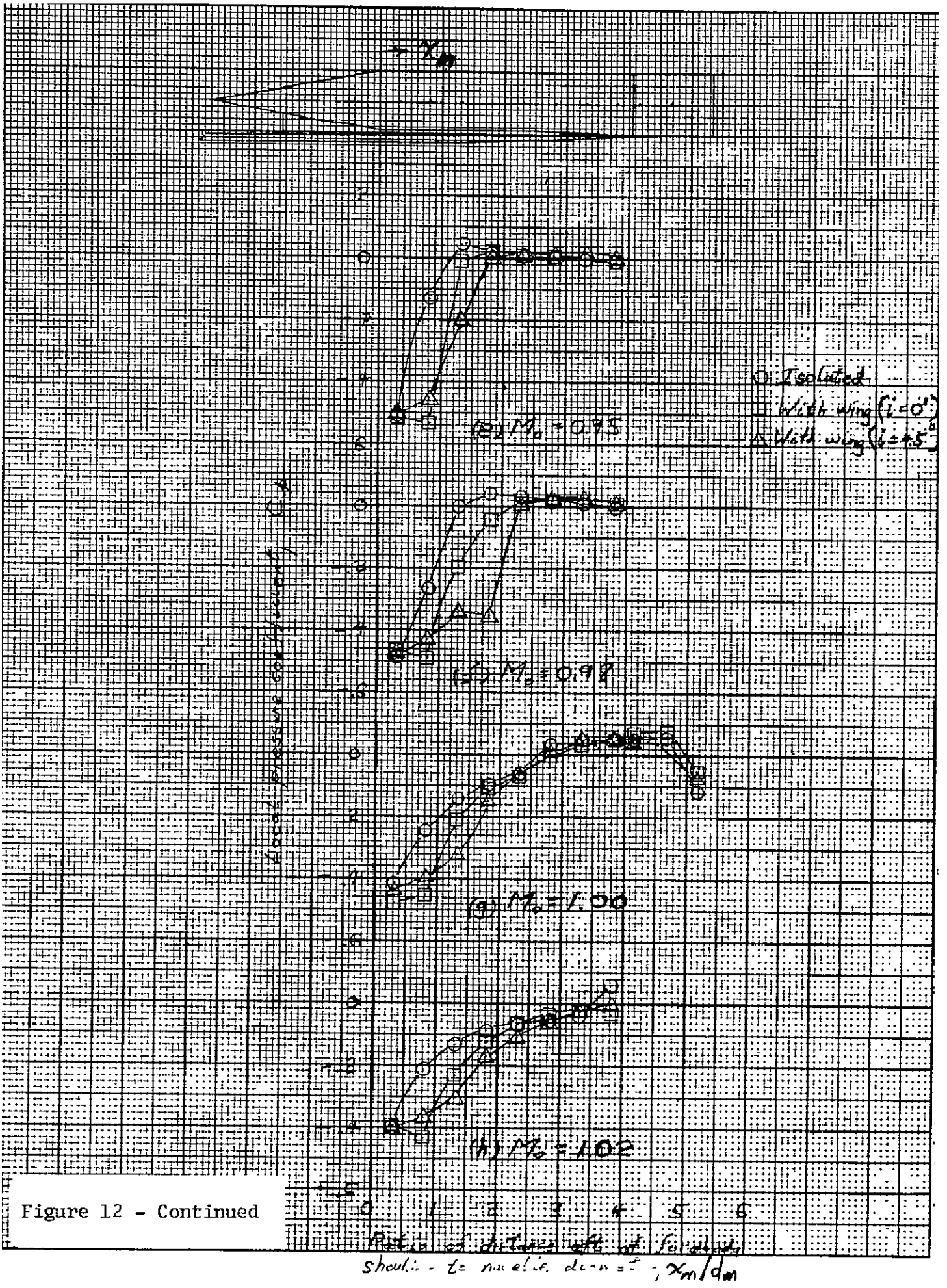

Figure 12 - Continued

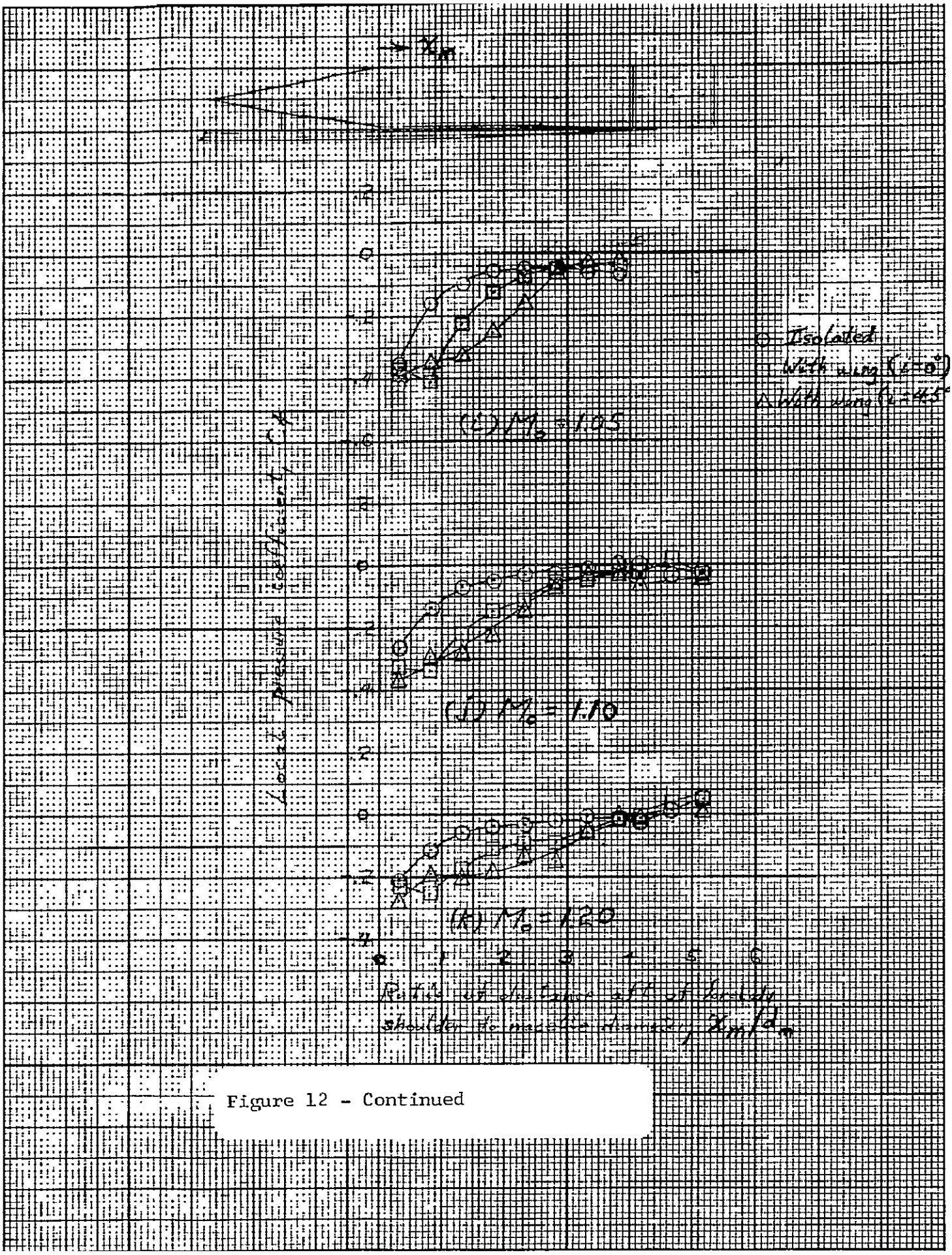

Figure 12 - Continued

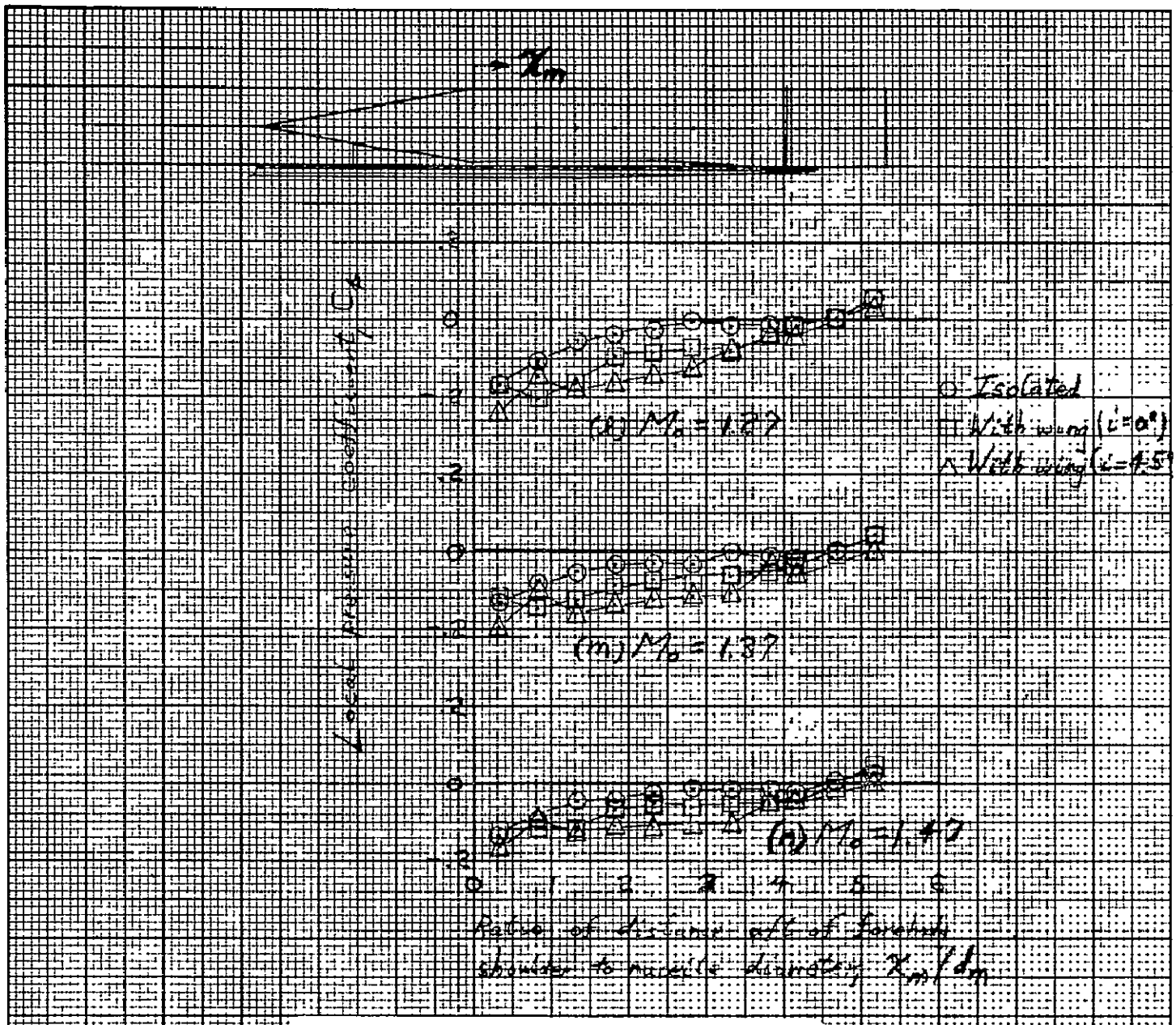

Figure 12 - Concluded

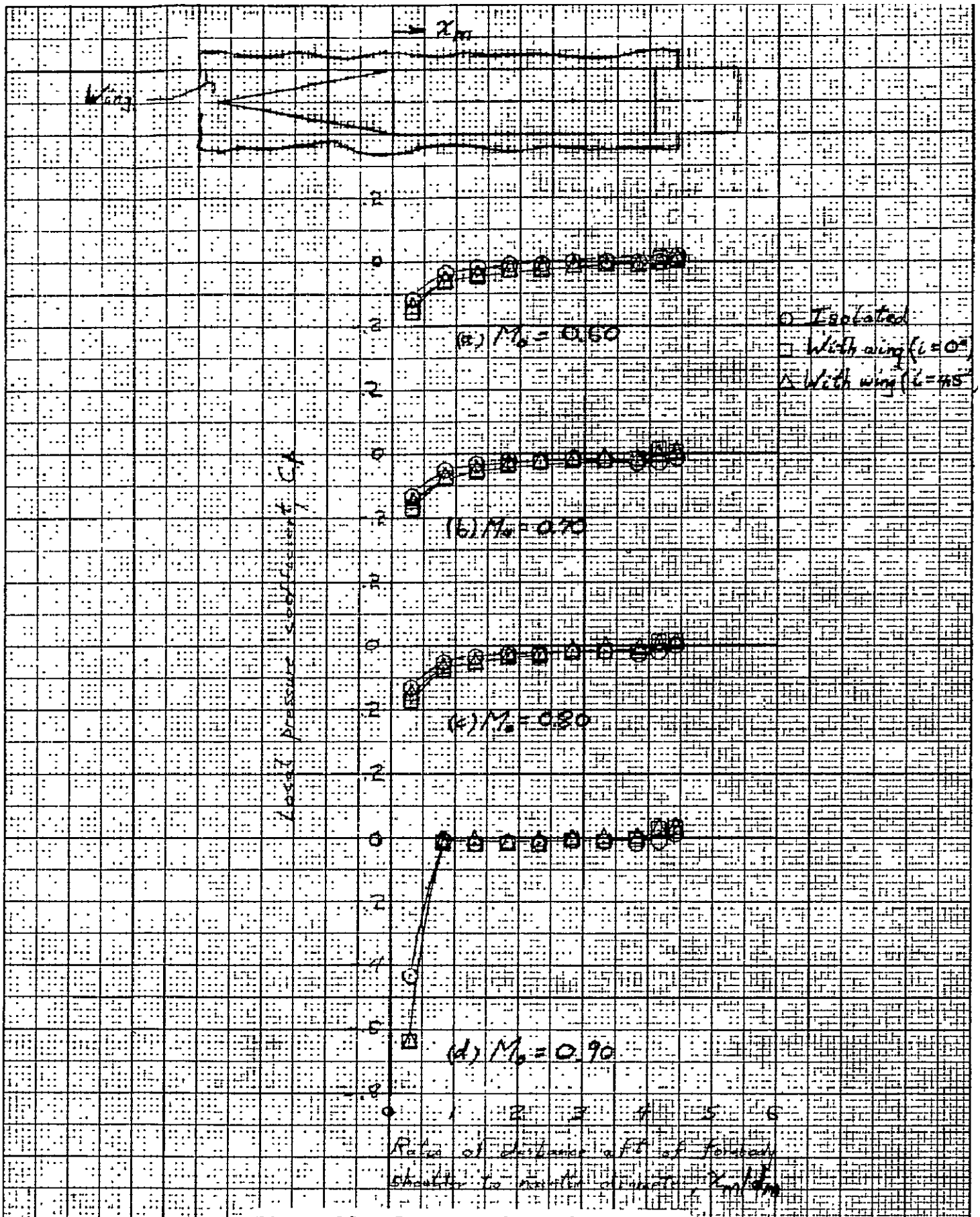

Figure 13 - Pressure distributions along vertical centerline of nacelle; Cylindrical afterbody

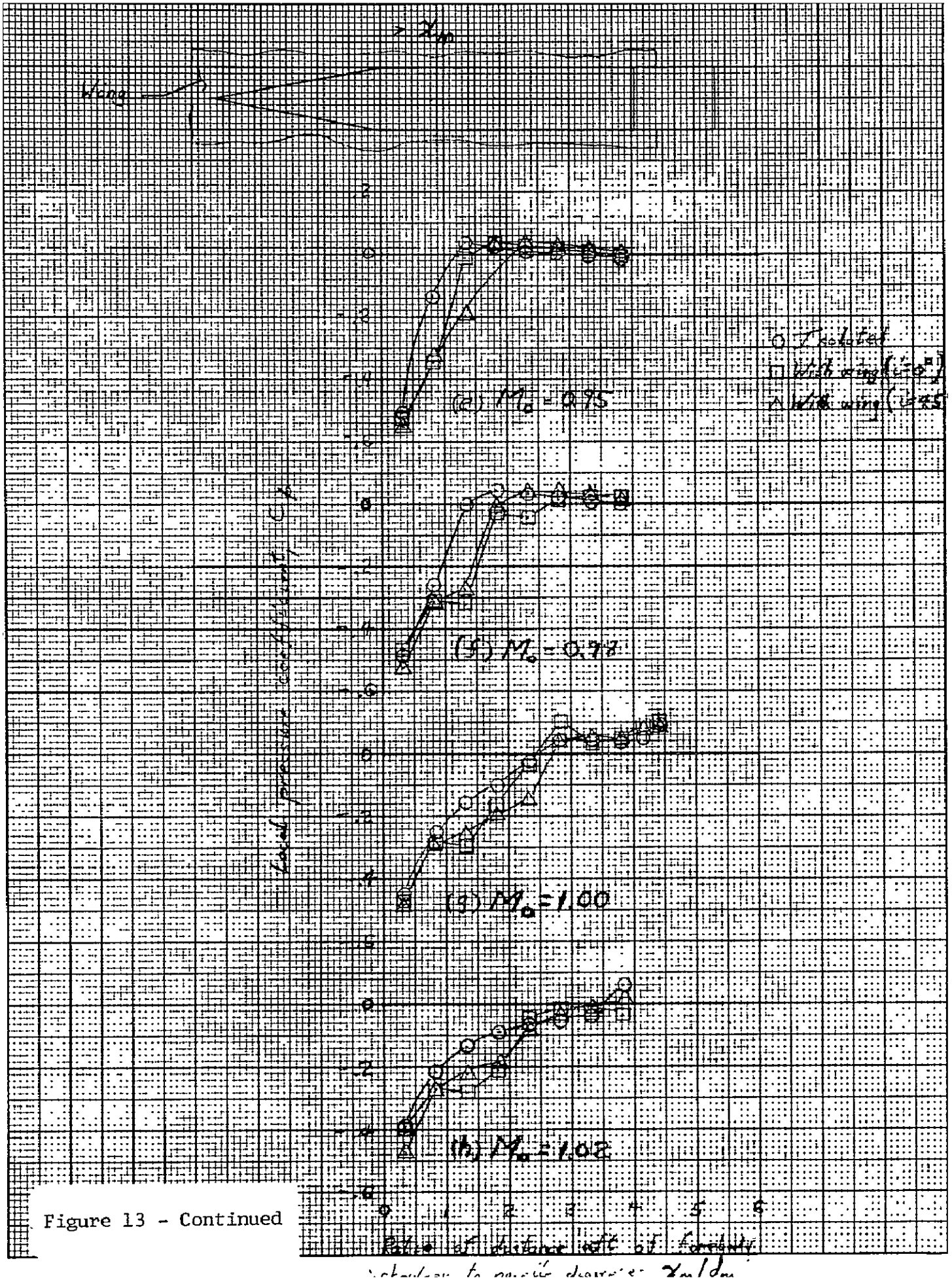

Figure 13 - Continued

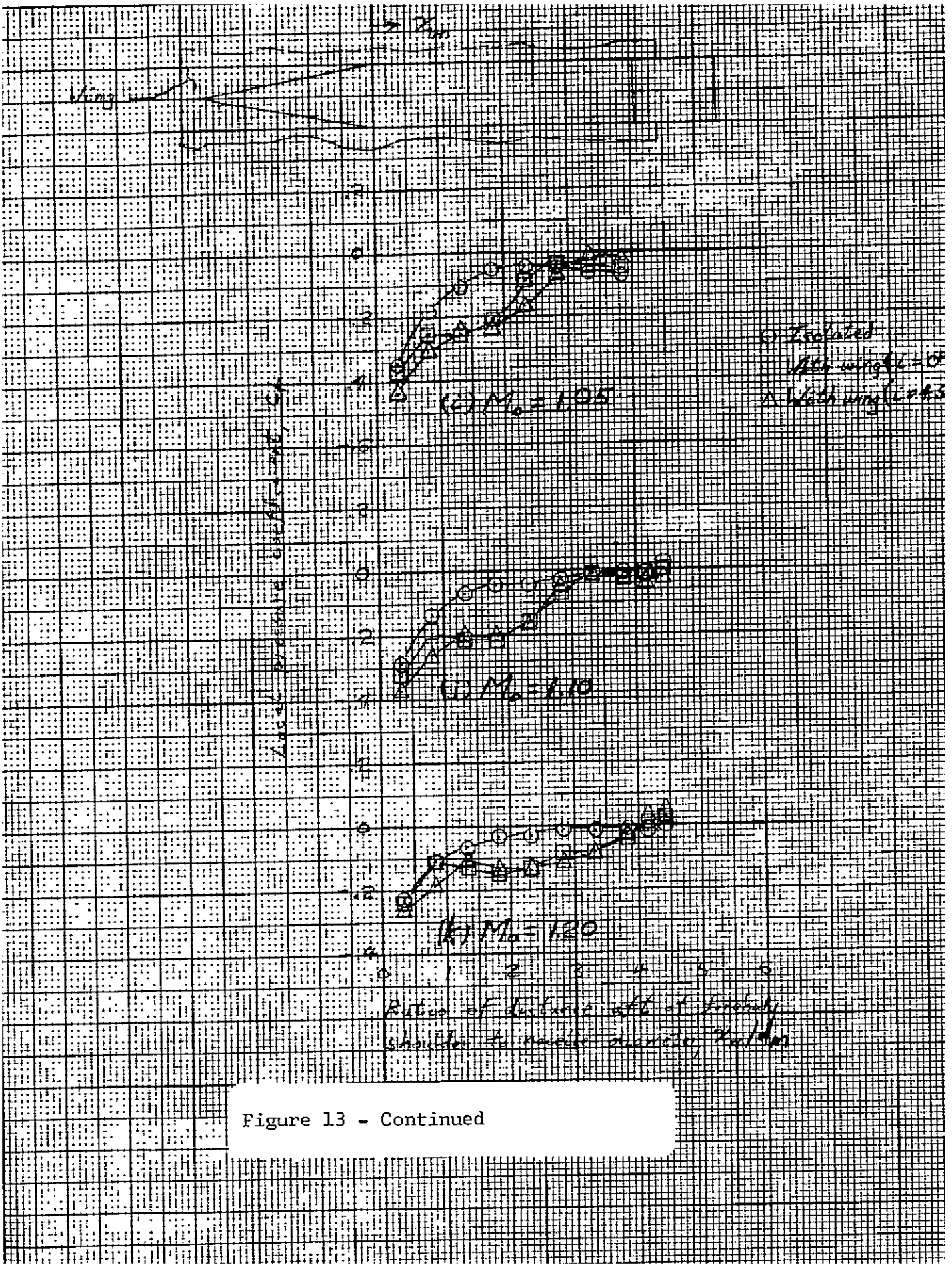

Figure 13 - Continued

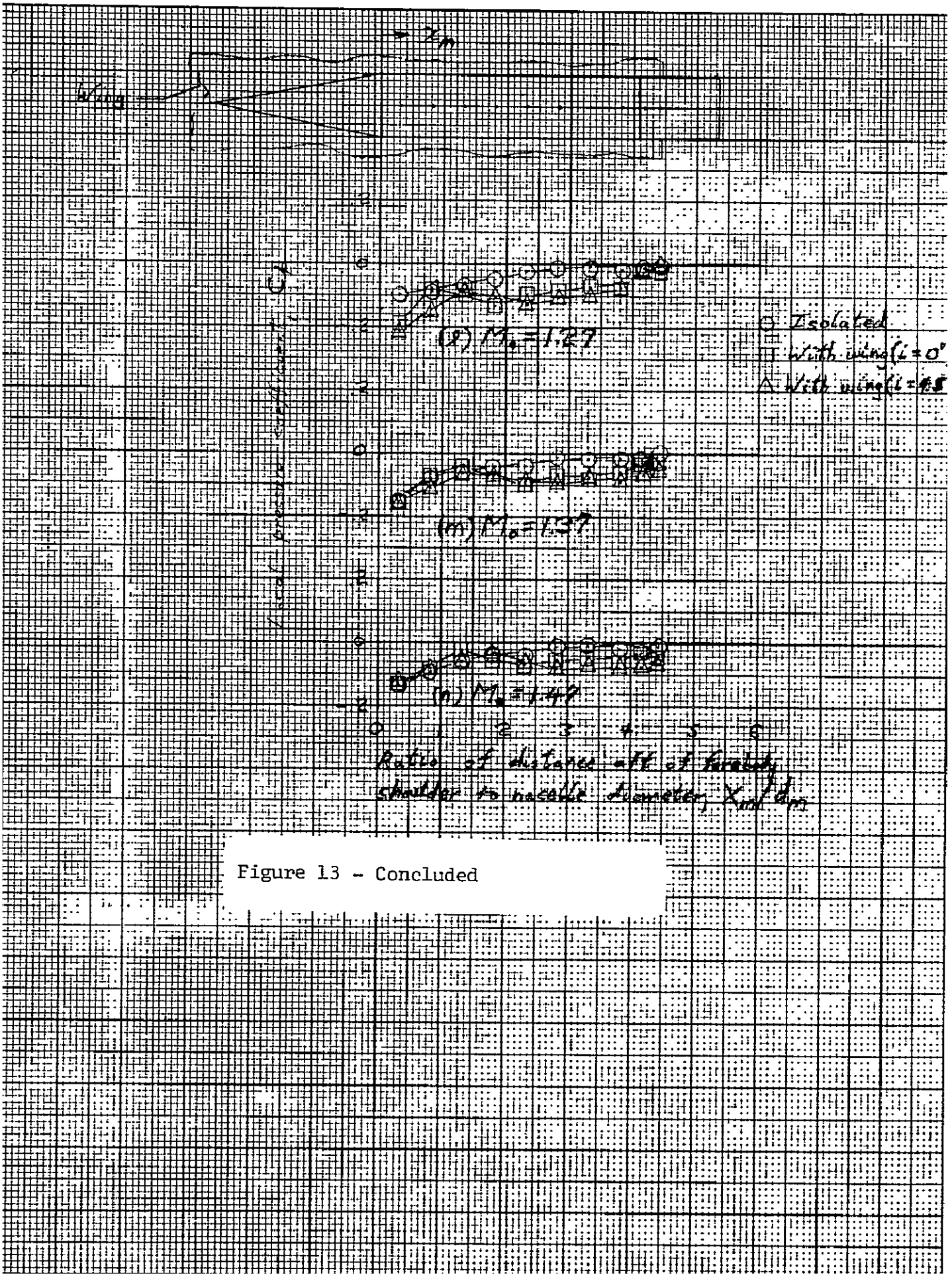

Figure 13 - Concluded

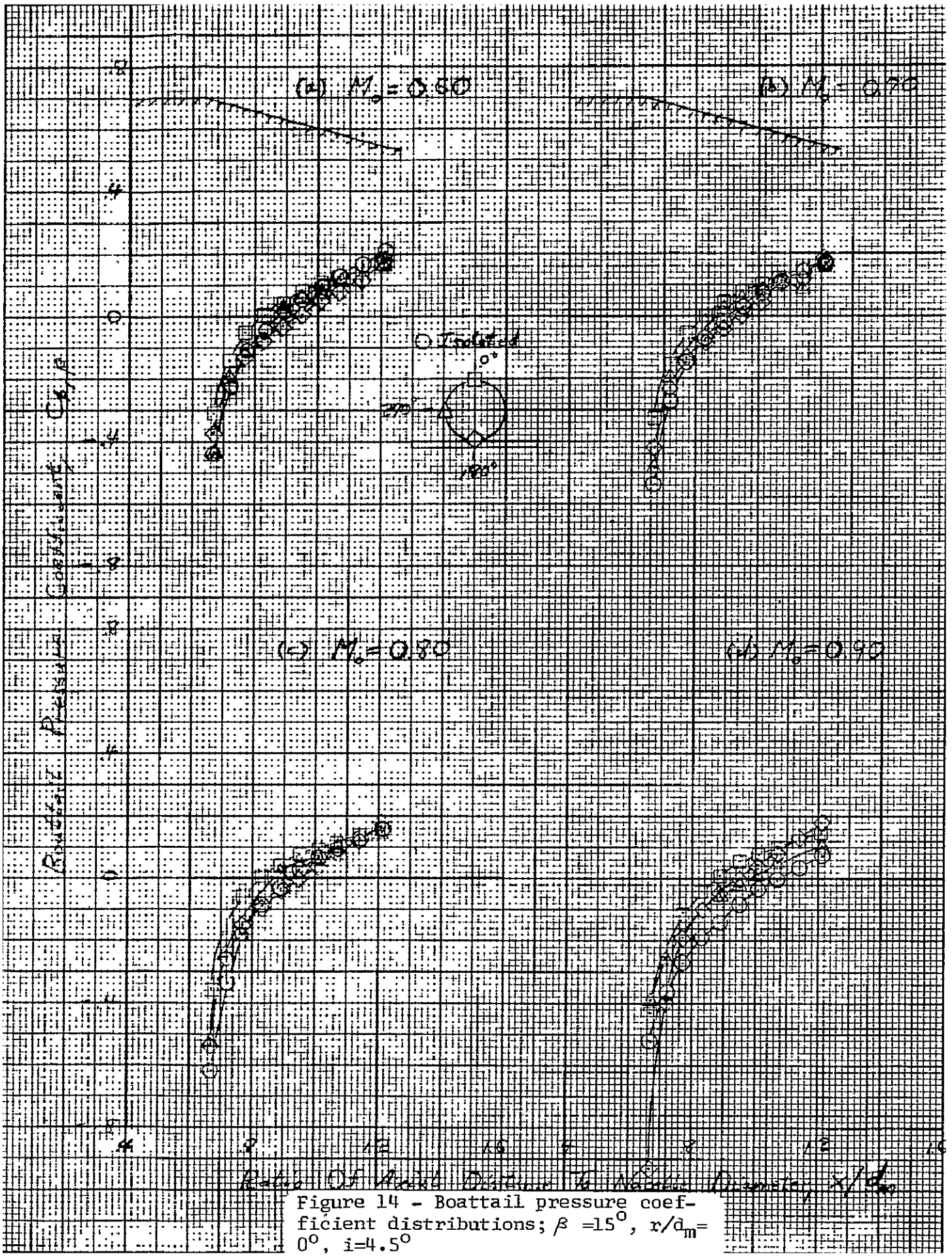

Figure 14 - Boattail pressure coefficient distributions; β =15°, x/d_m= 0°, i=4.5°

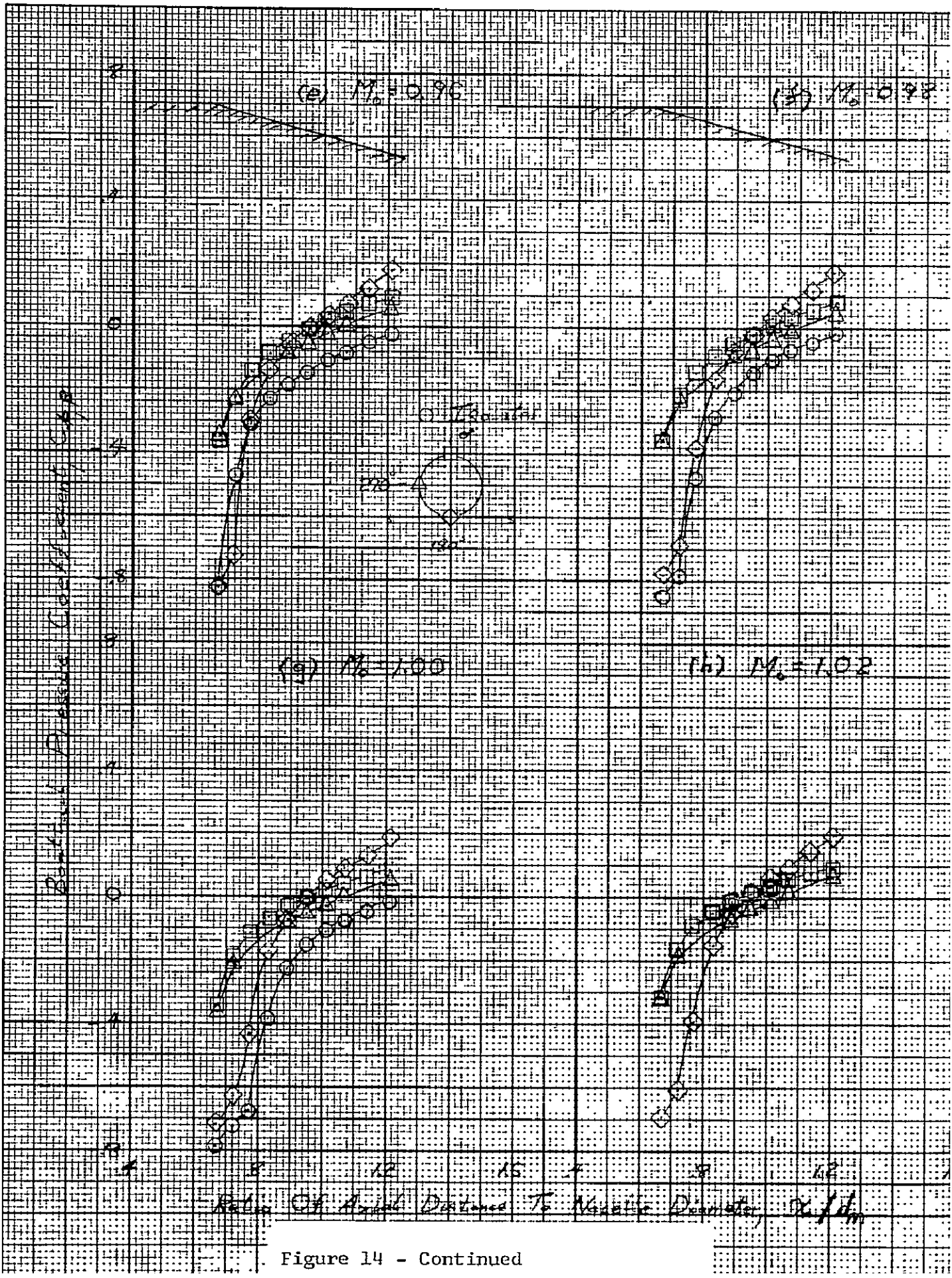

Figure 14 - Continued

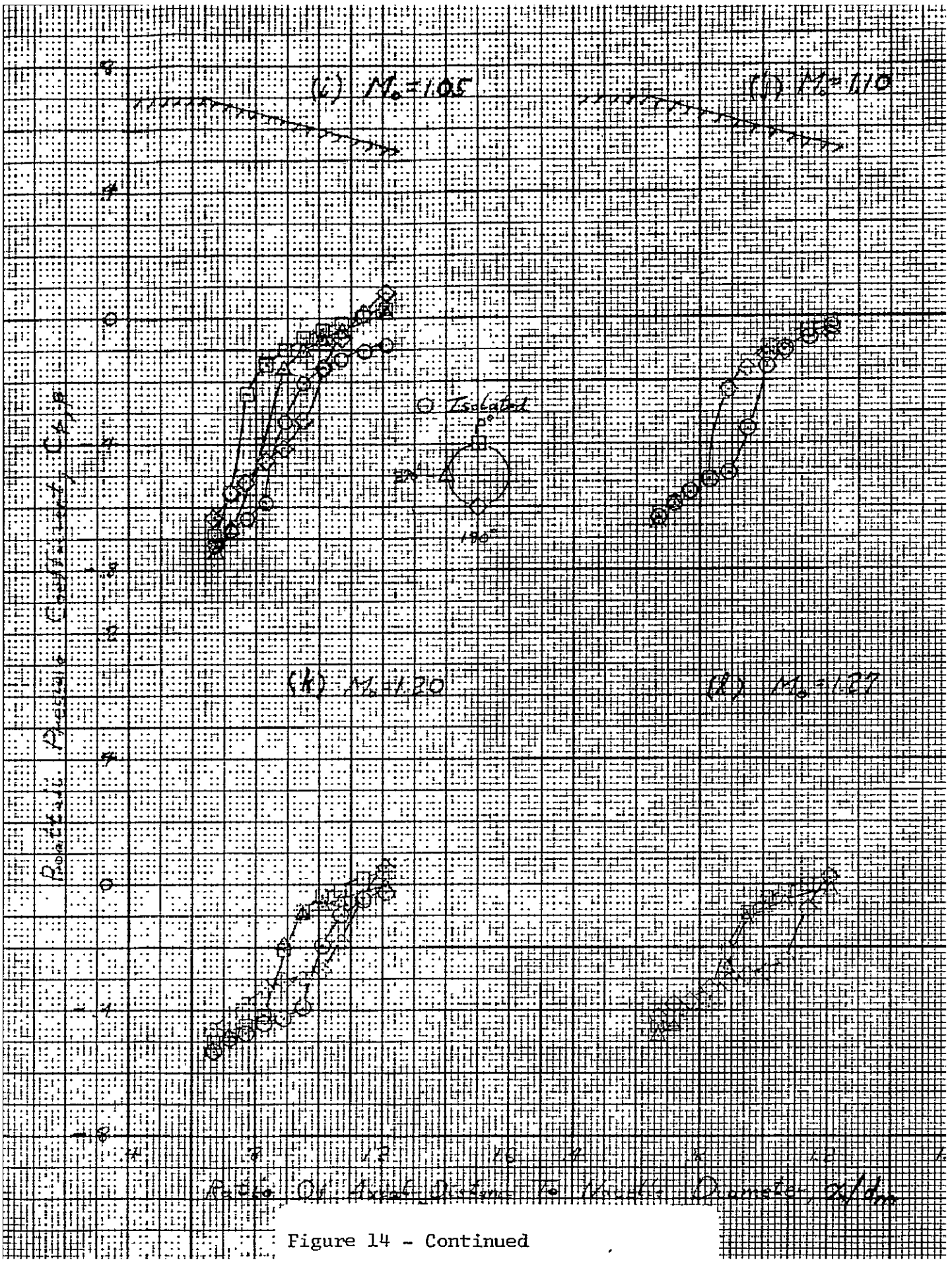

Figure 14 - Continued

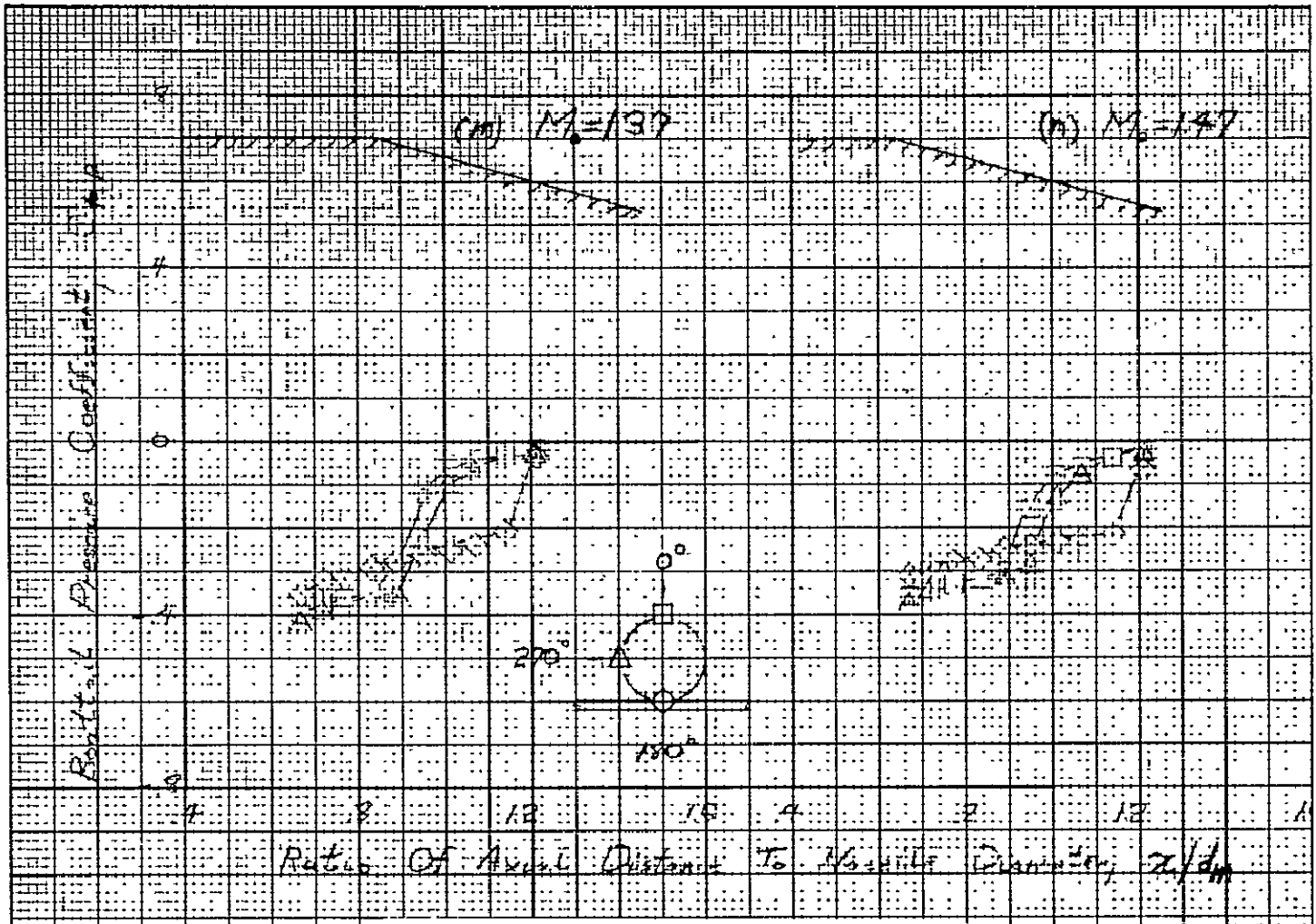

Figure 14 - Concluded

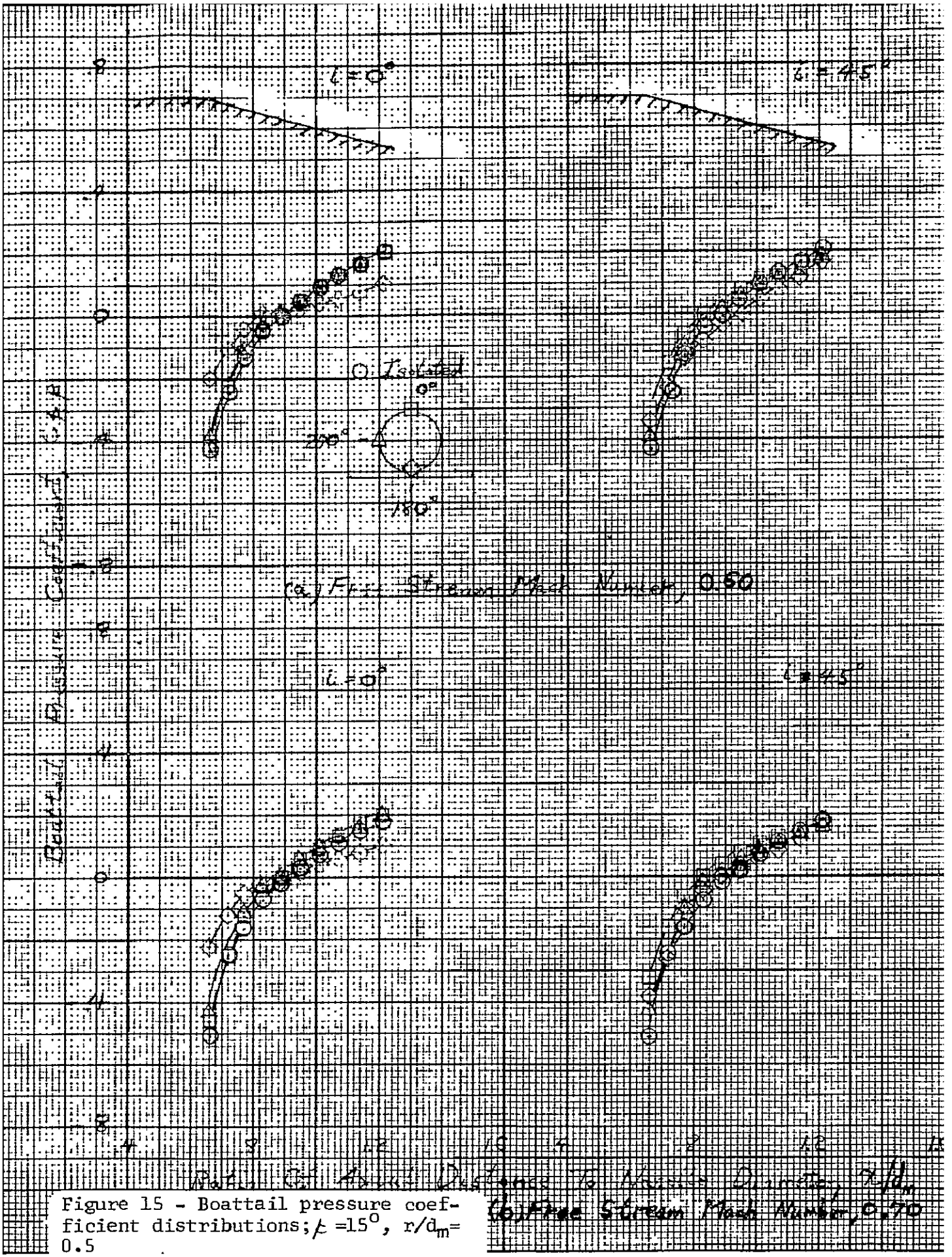

Figure 15 - Boattail pressure coefficient distributions; $\alpha = 15°$, $r/d_m = 0.5$

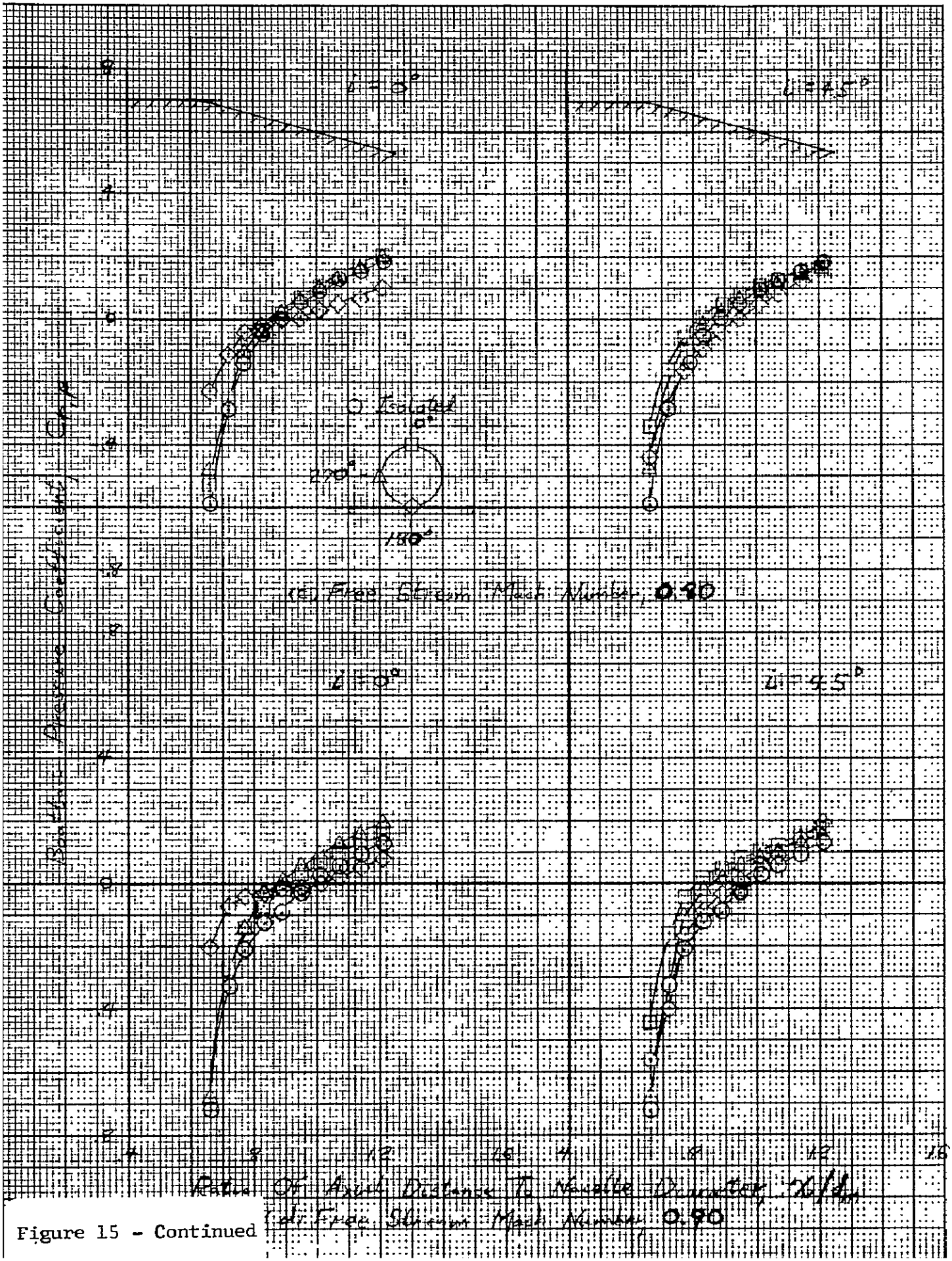

Figure 15 - Continued

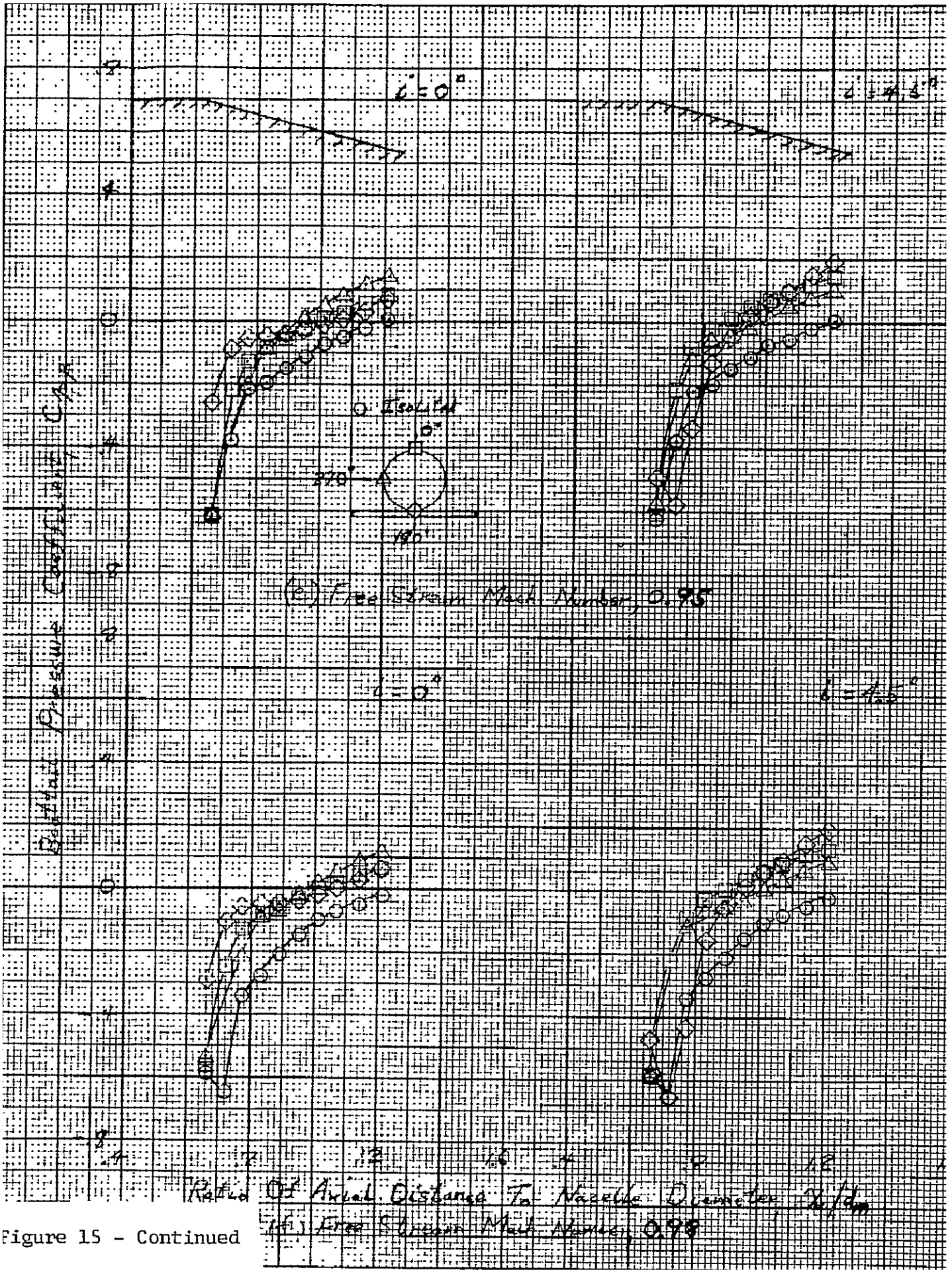

Figure 15 - Continued

Figure 15 - Continued

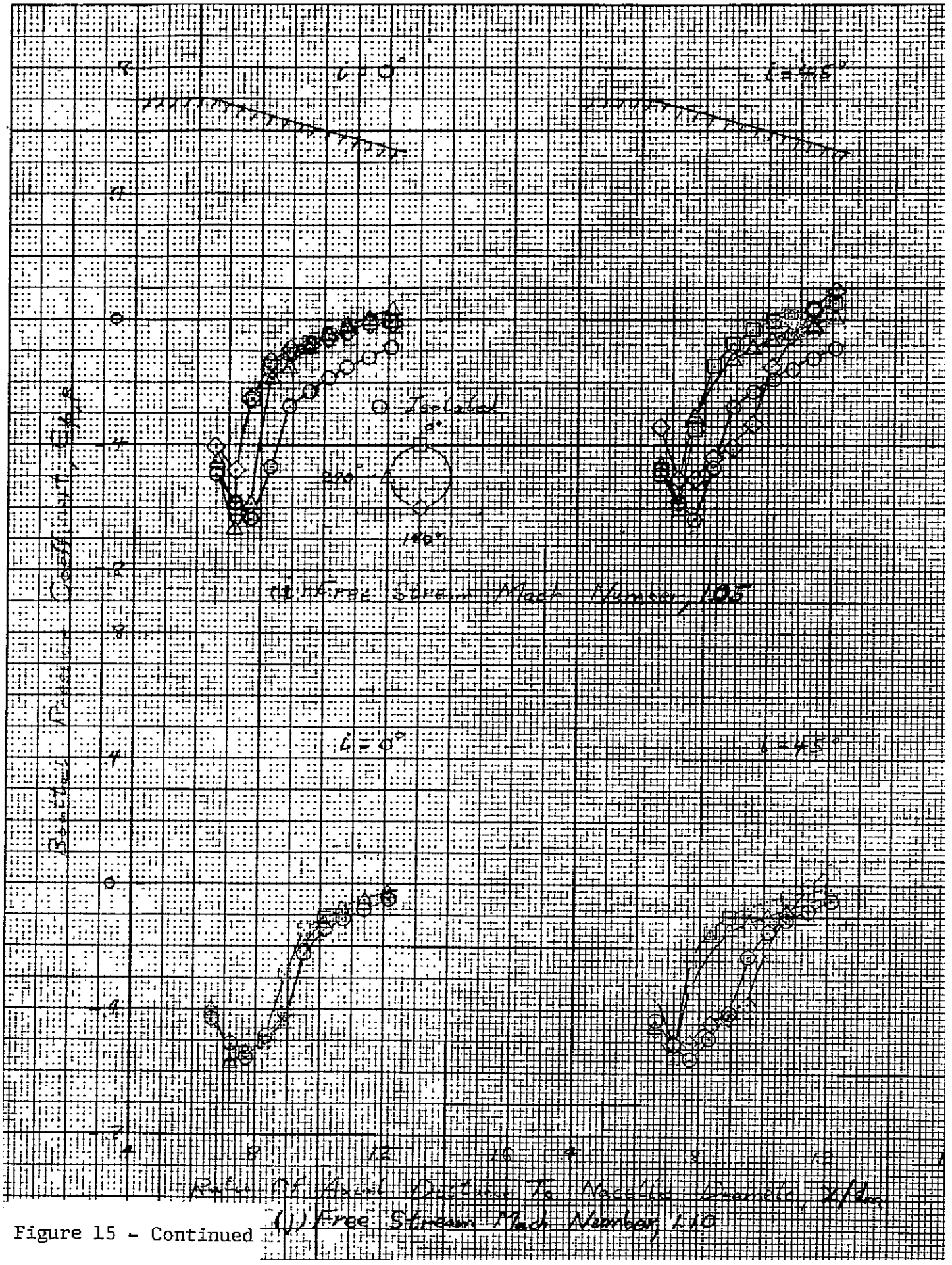

Figure 15 - Continued

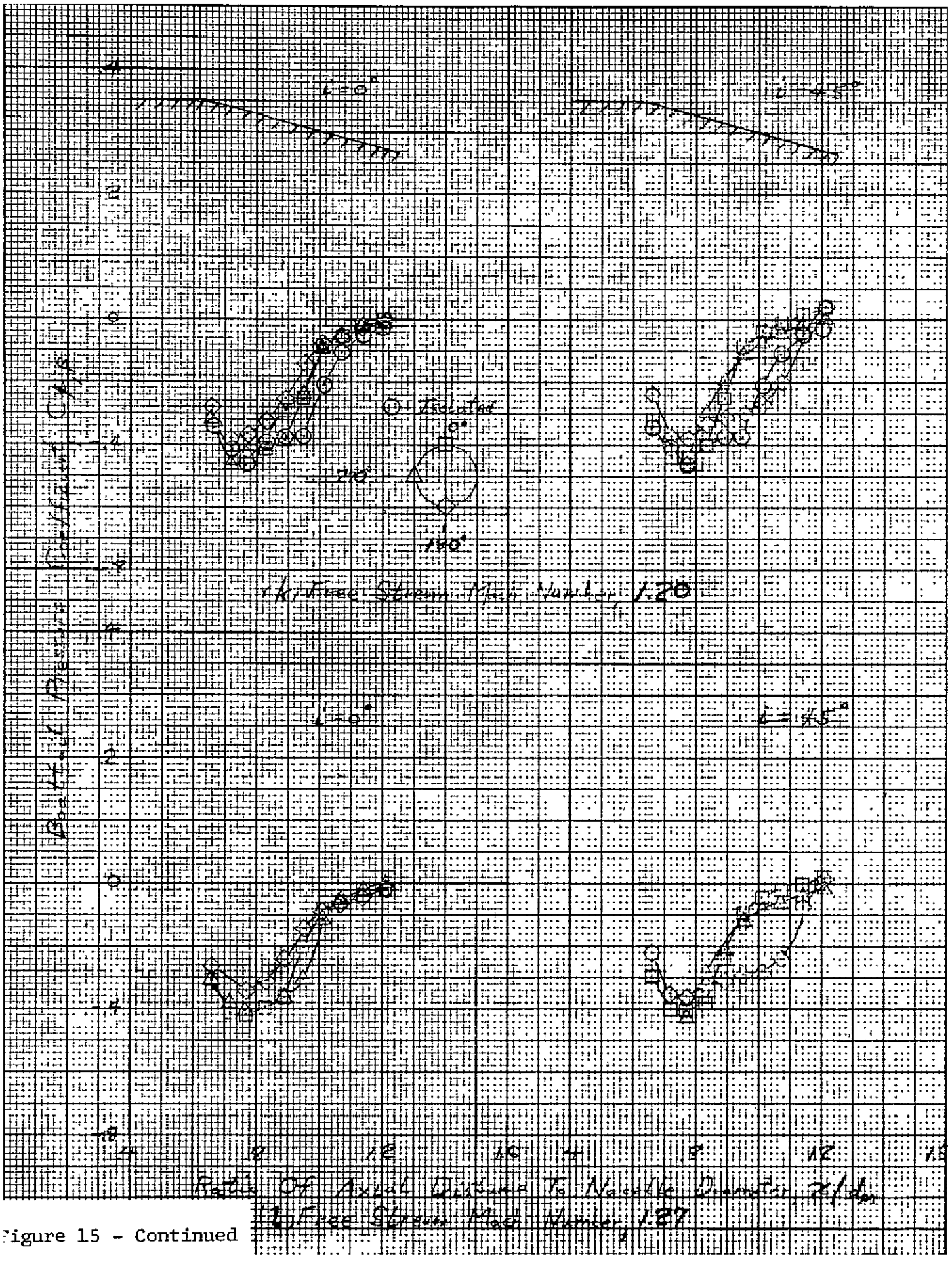

Figure 15 - Continued

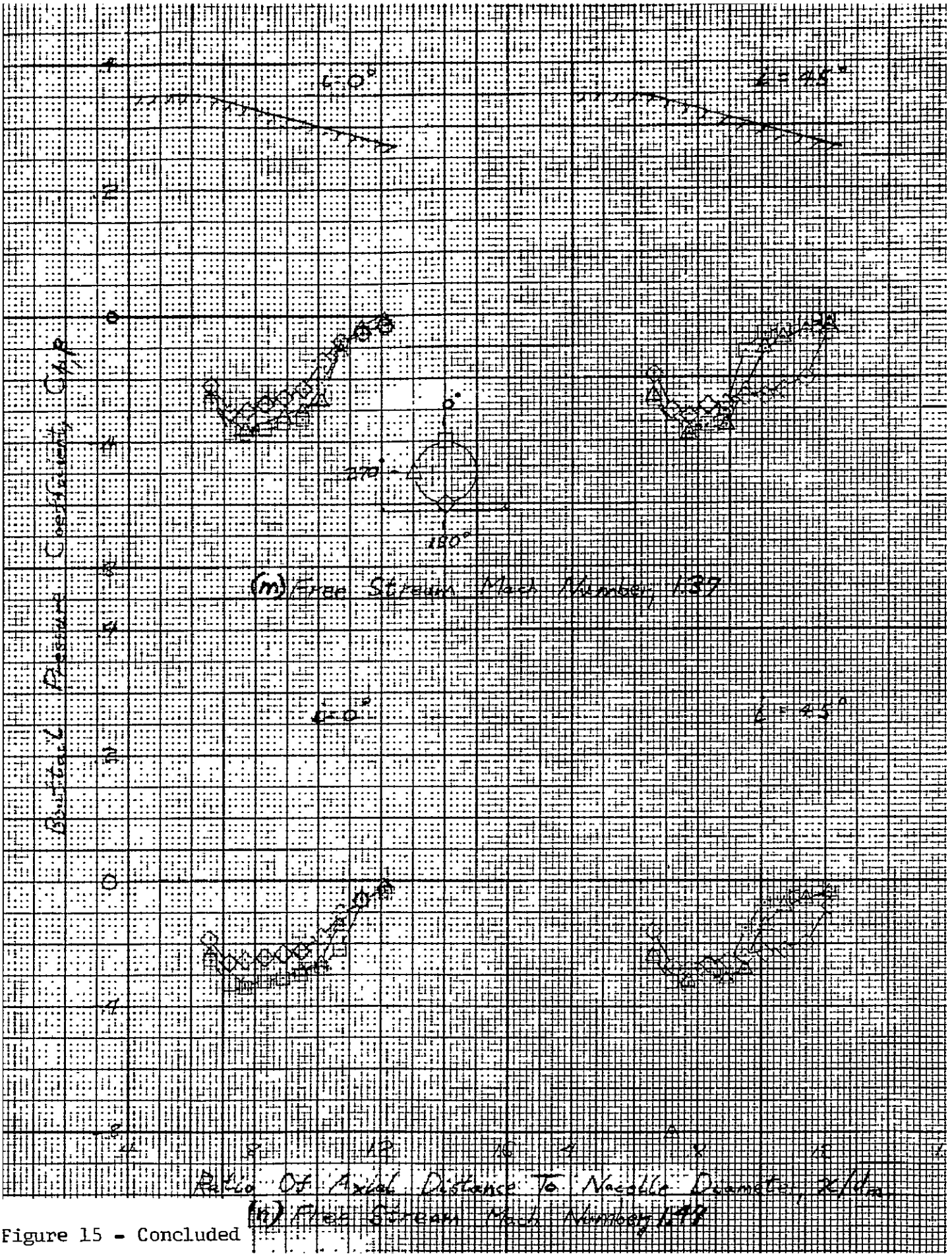

Figure 15 - Concluded

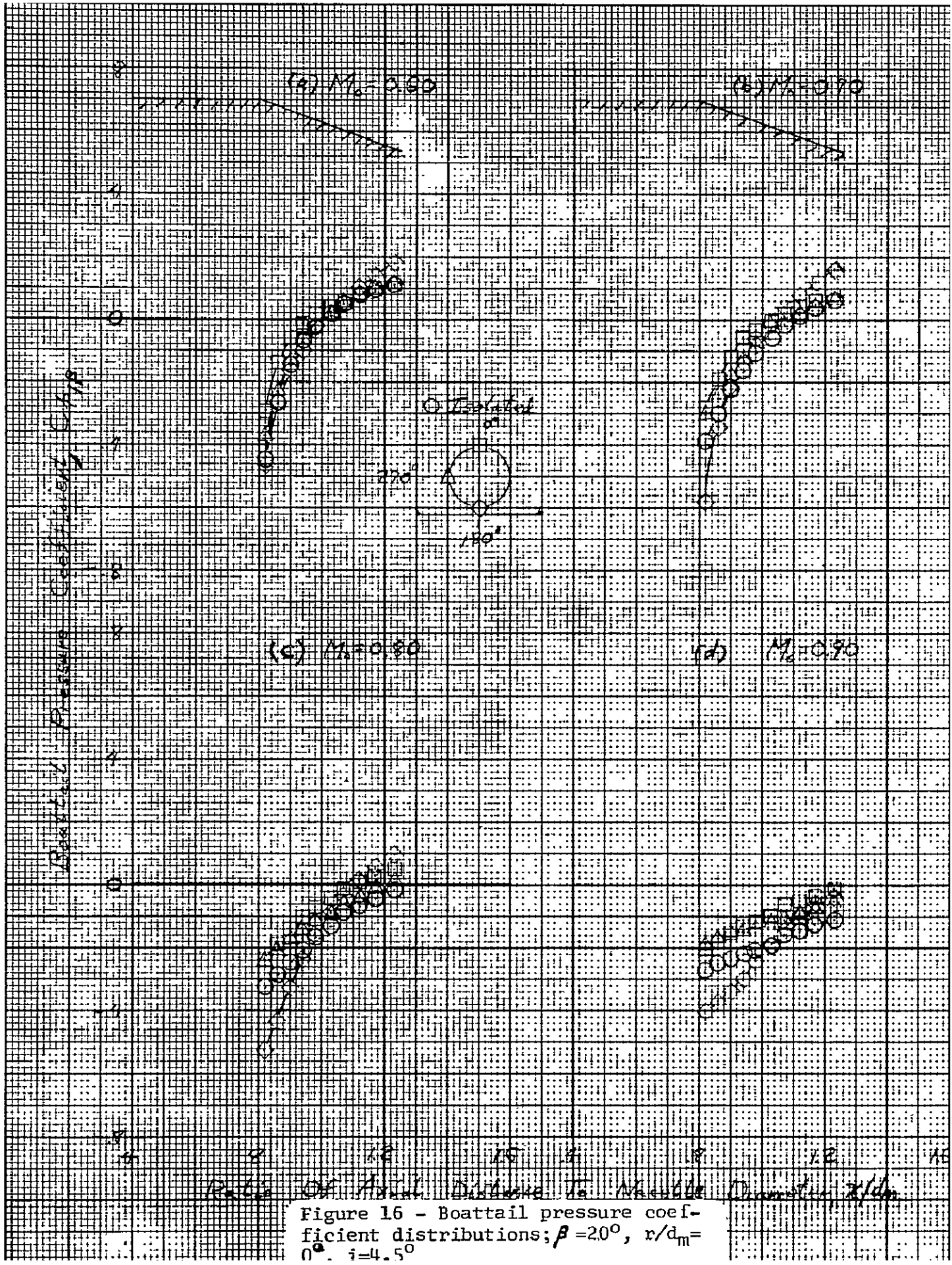

Figure 16 - Boattail pressure coefficient distributions; $\beta = 20^{\circ}$, $r/d_m = 0^{a}$, $i = 4.5^{\circ}$

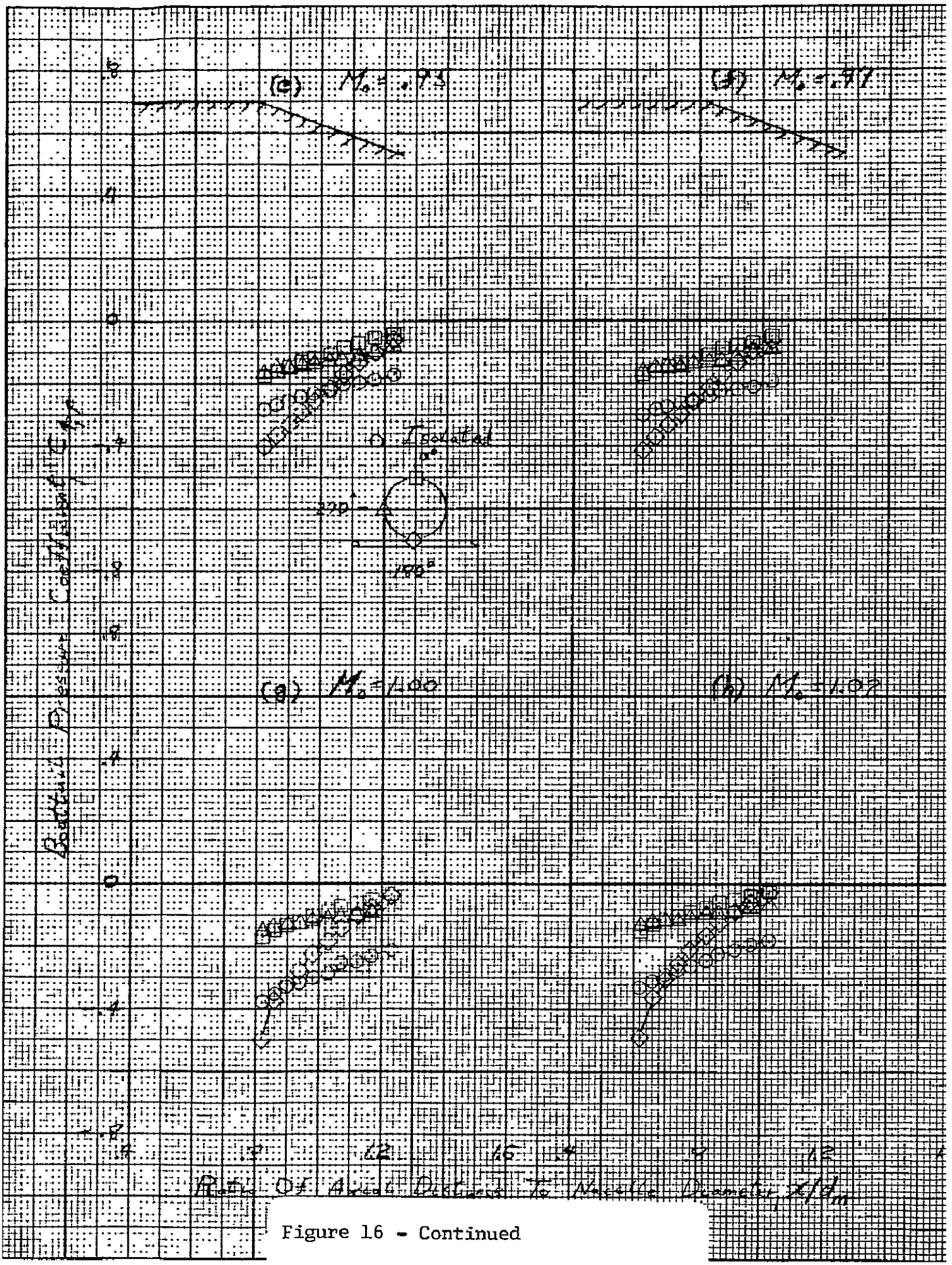

Figure 16 - Continued

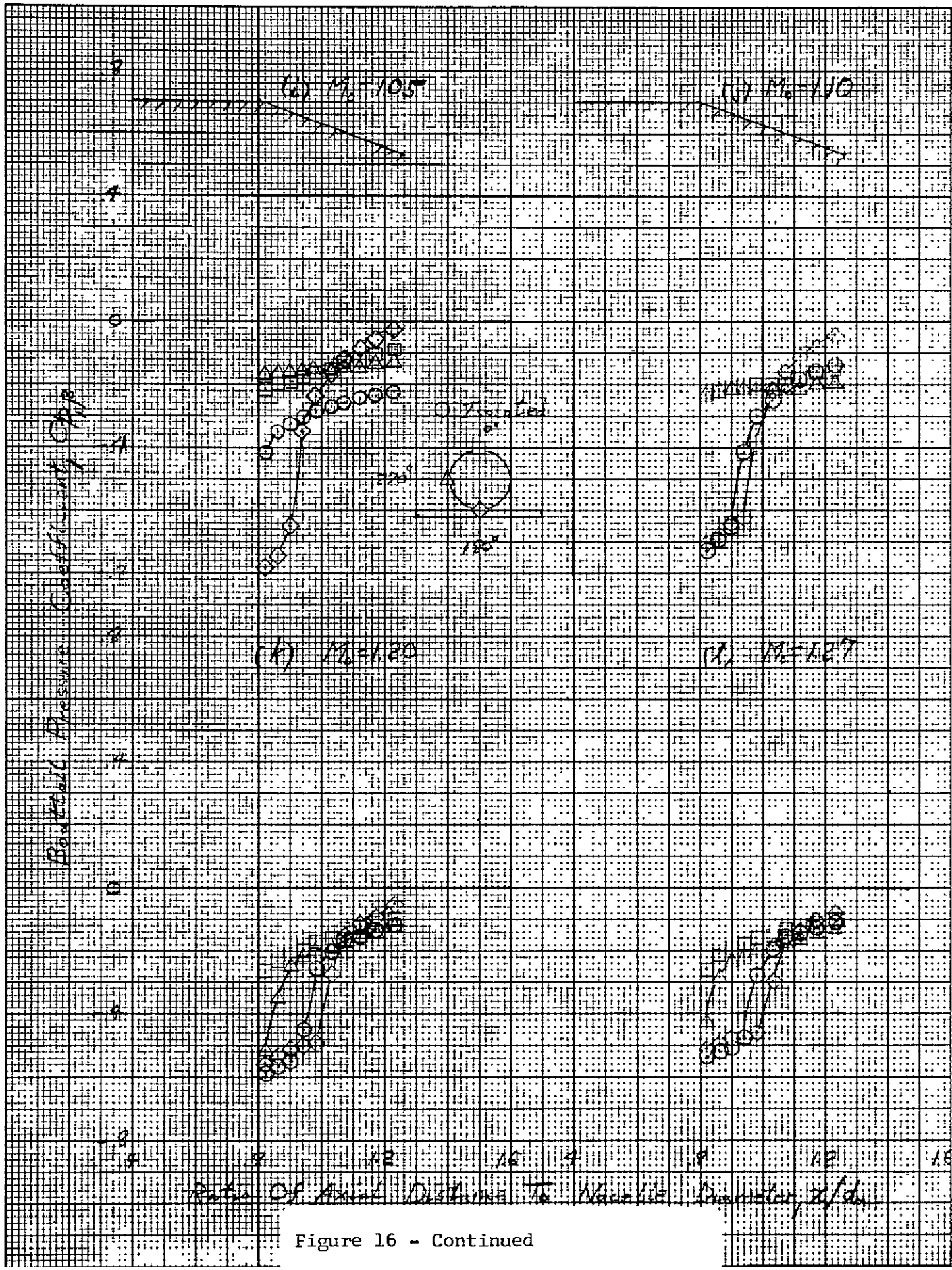

Figure 16 - Continued

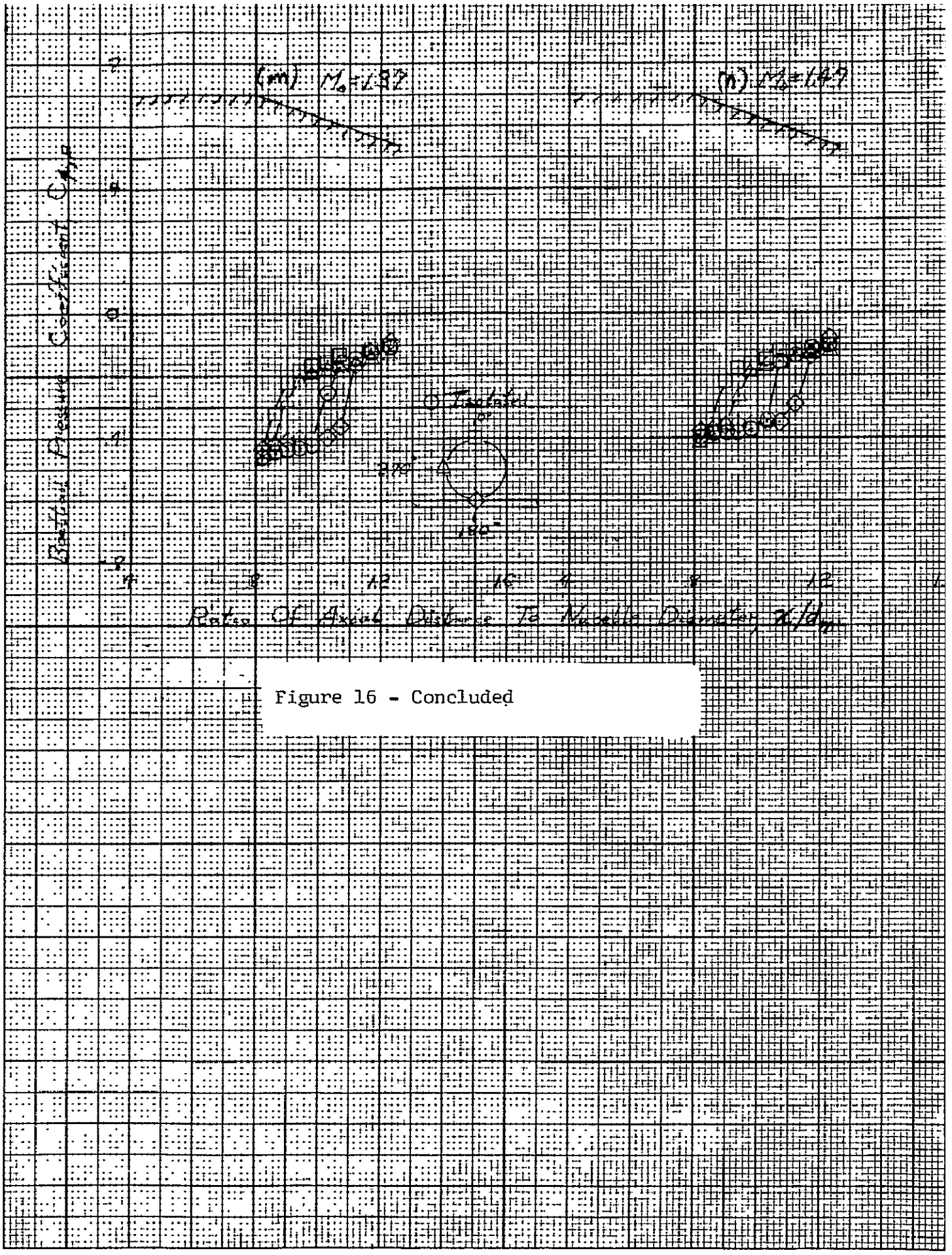

Figure 16 - Concluded

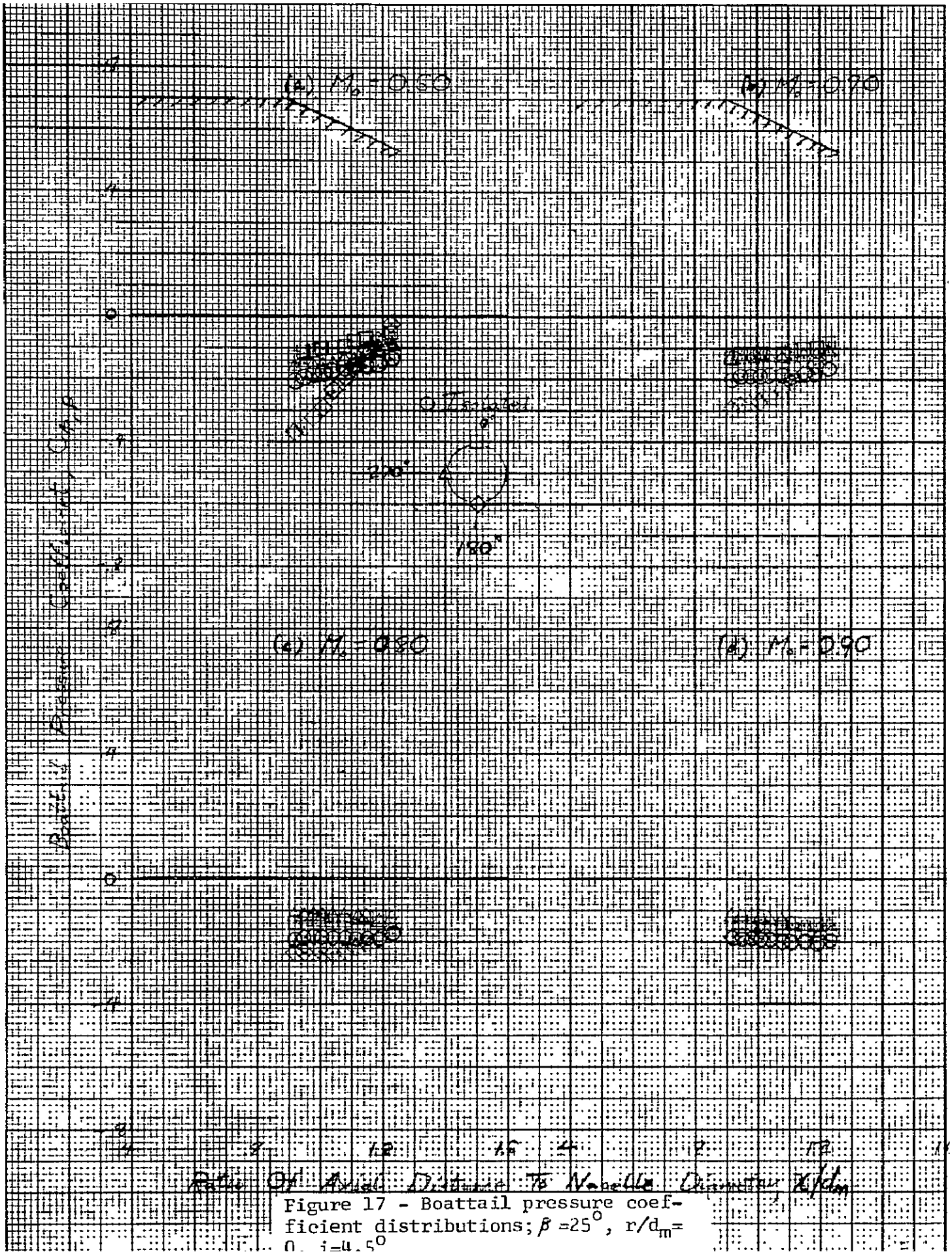

Figure 17 - Boattail pressure coefficient distributions; $\beta = 25^{\circ}$, $r/d_m = 0$, $i = 4.5^{\circ}$

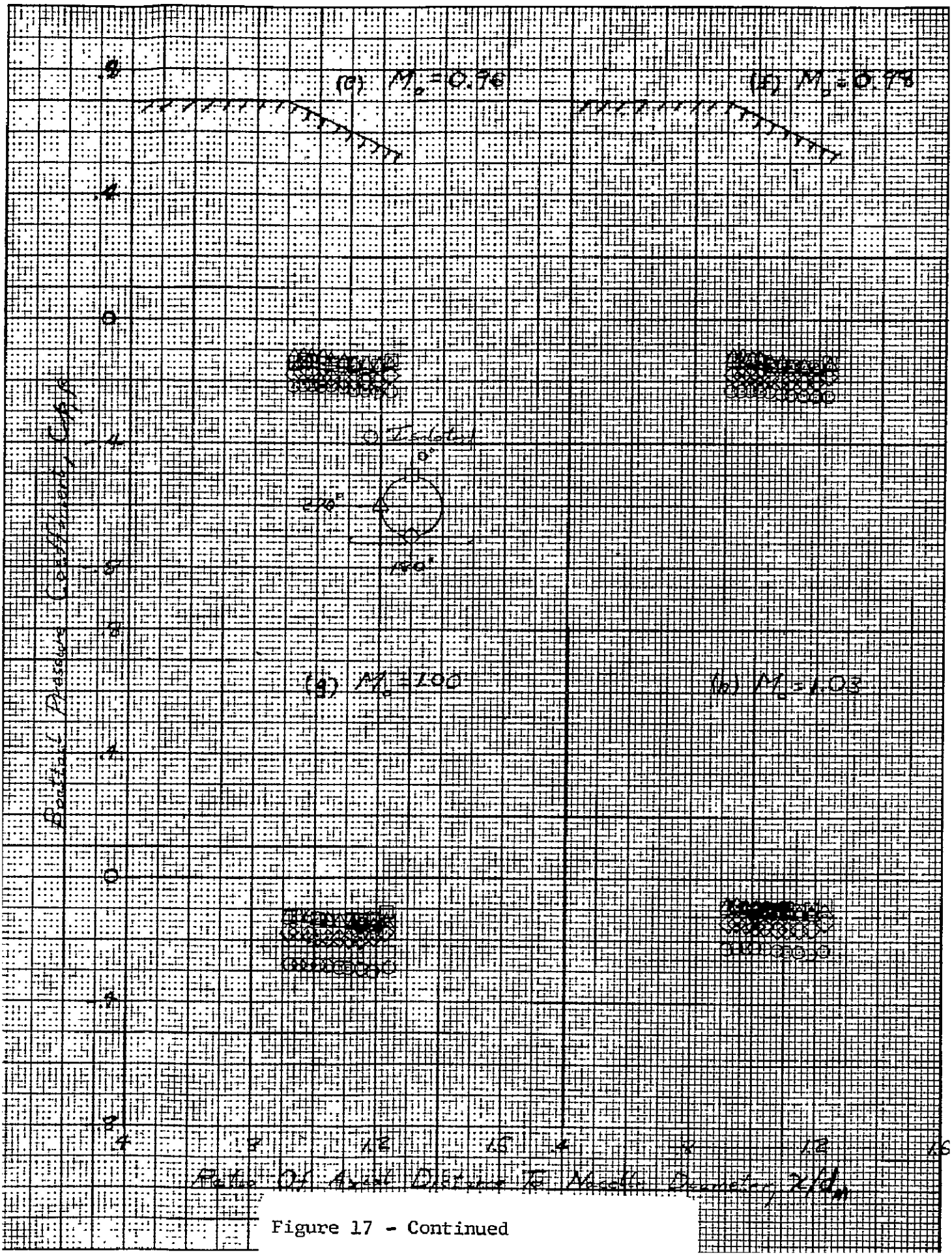

Figure 17 - Continued

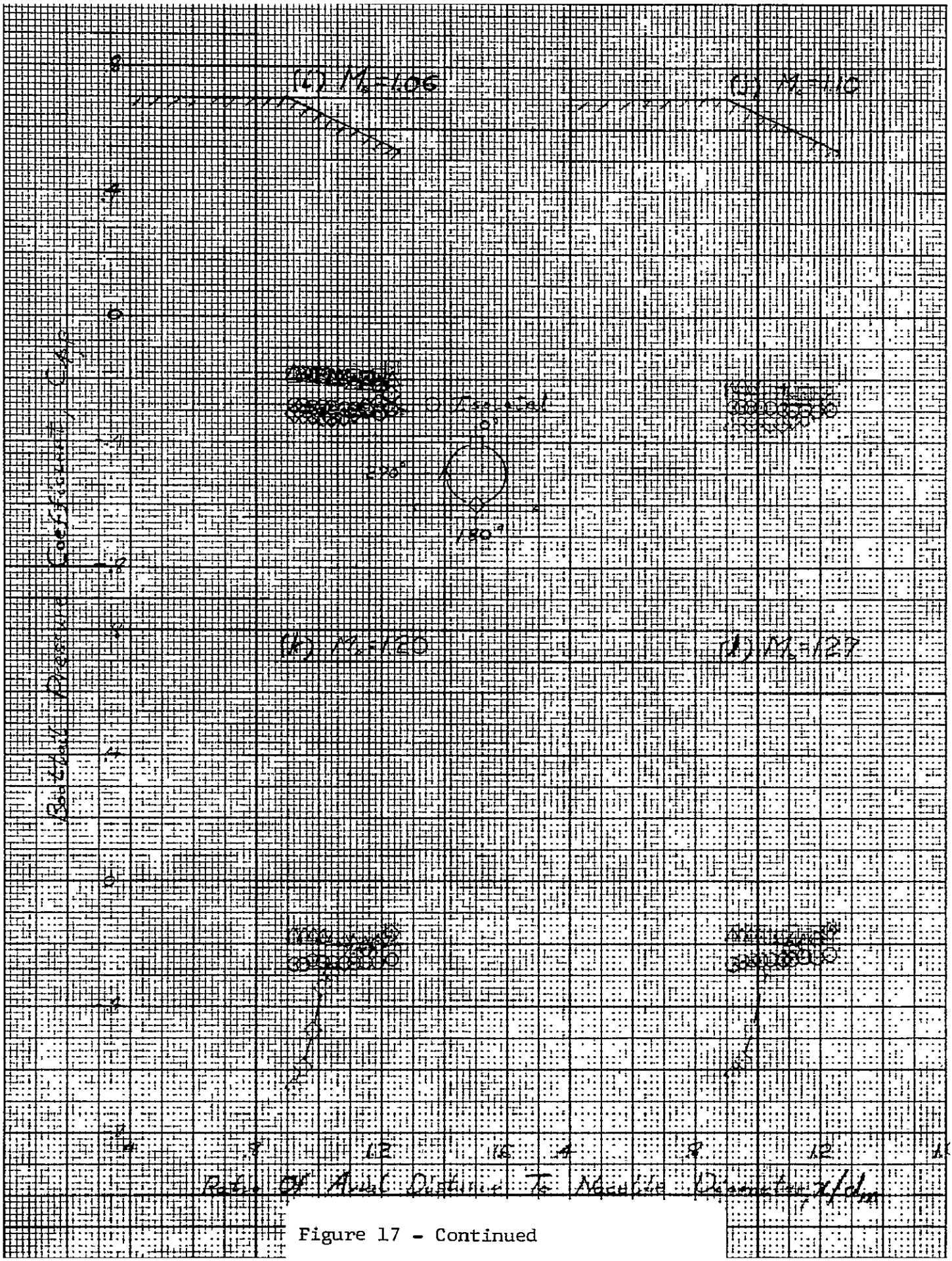

Figure 17 - Continued

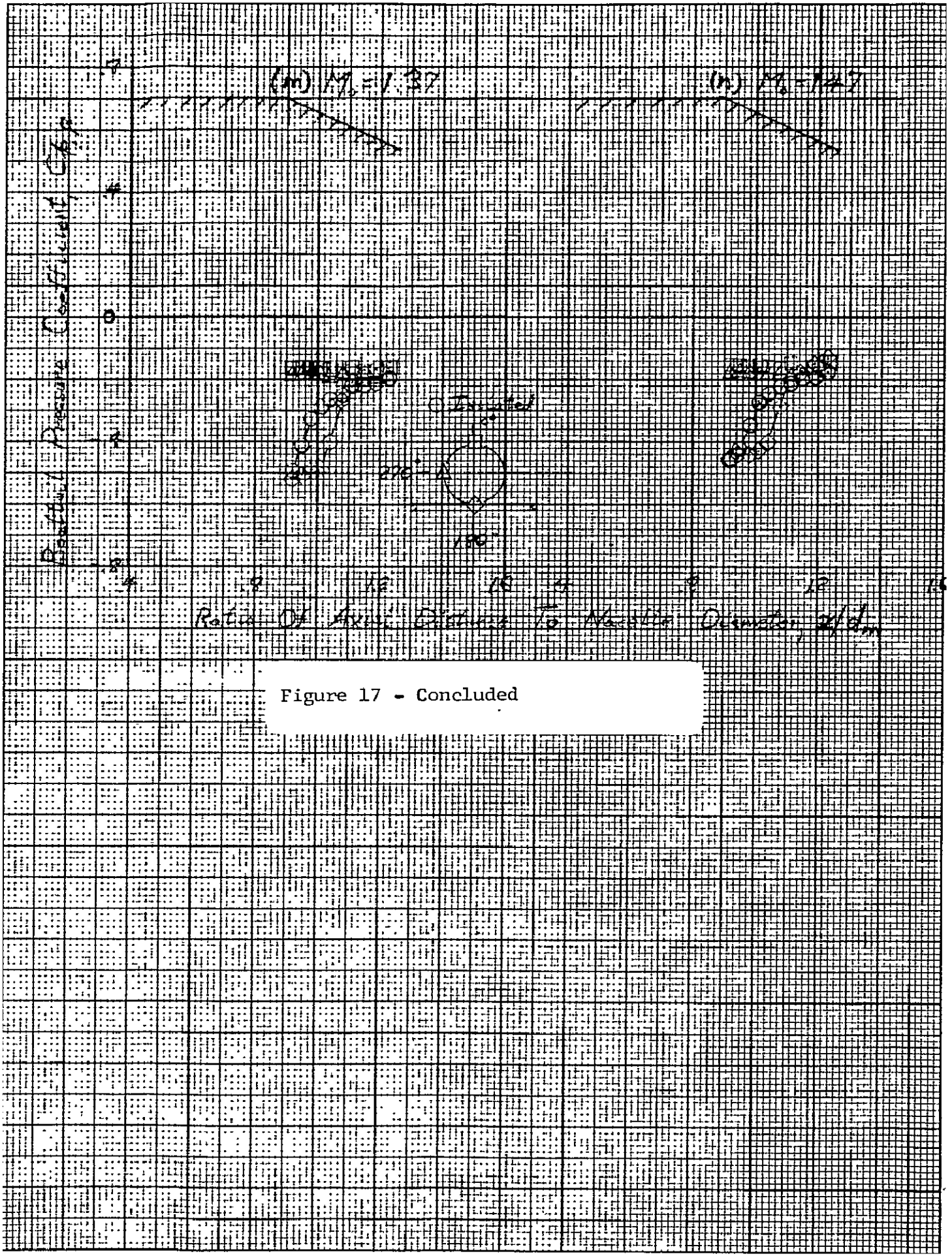

Figure 17 - Concluded

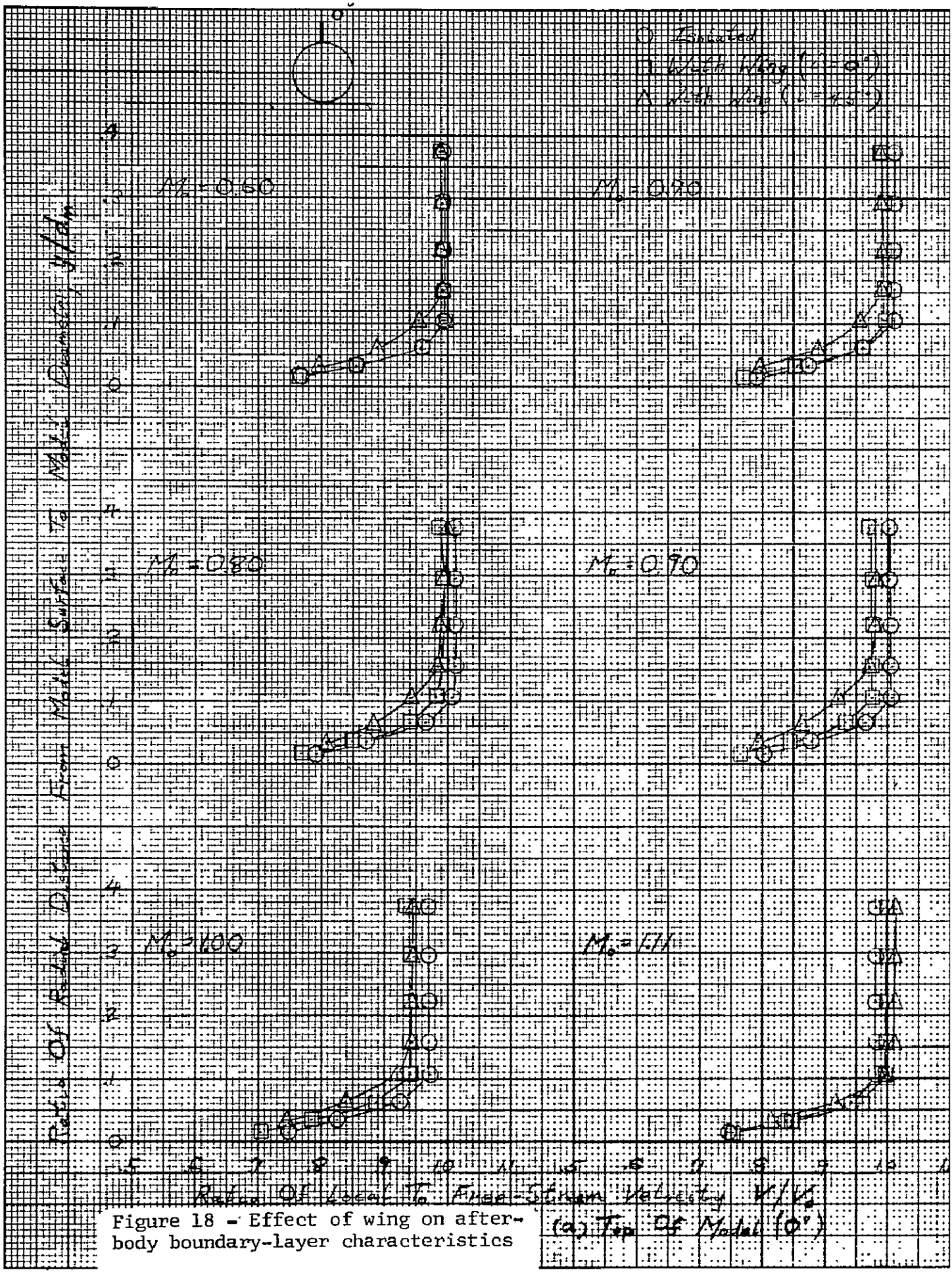

Figure 18 - Effect of wing on after-body boundary-layer characteristics

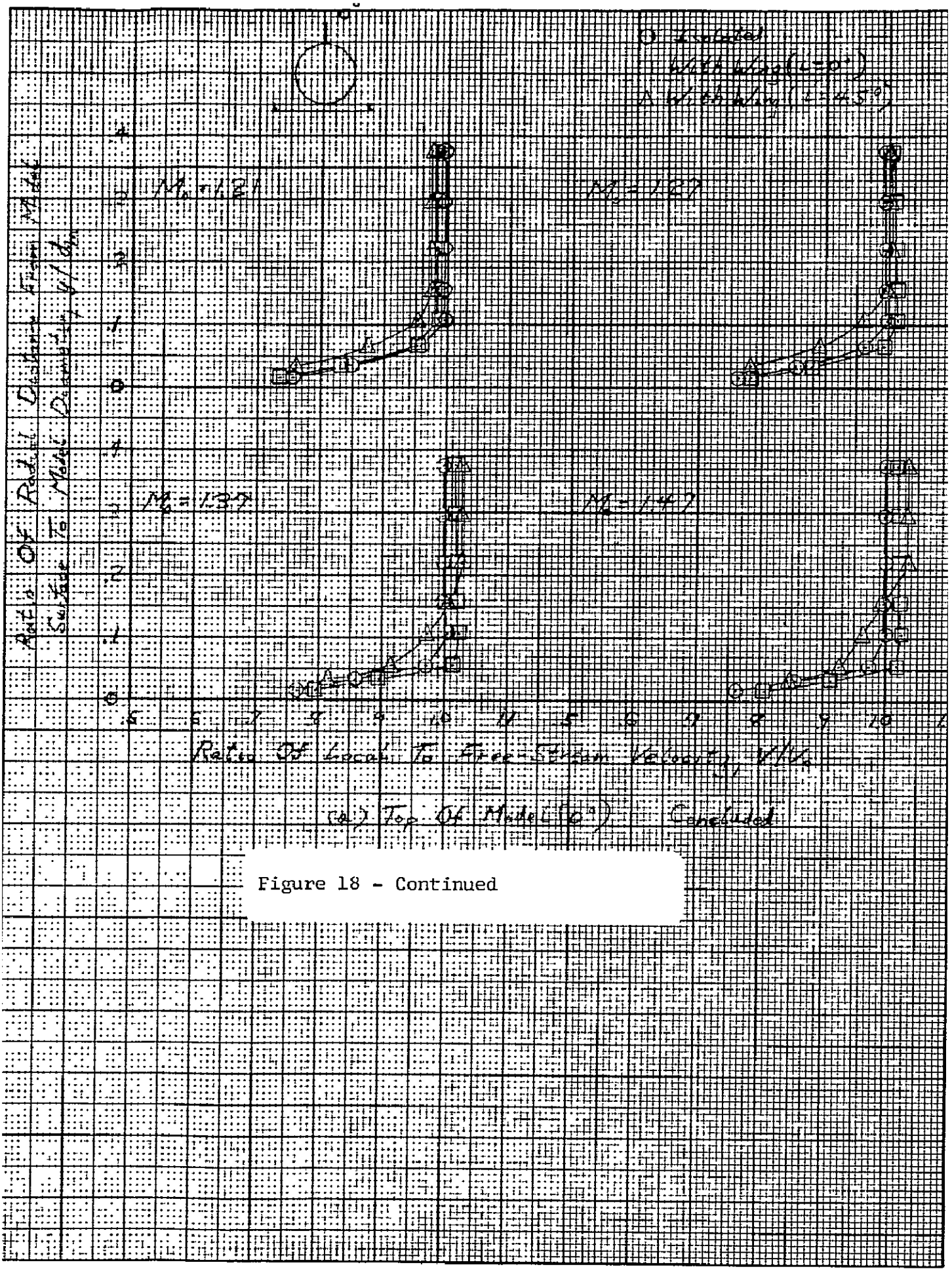

Figure 18 - Continued

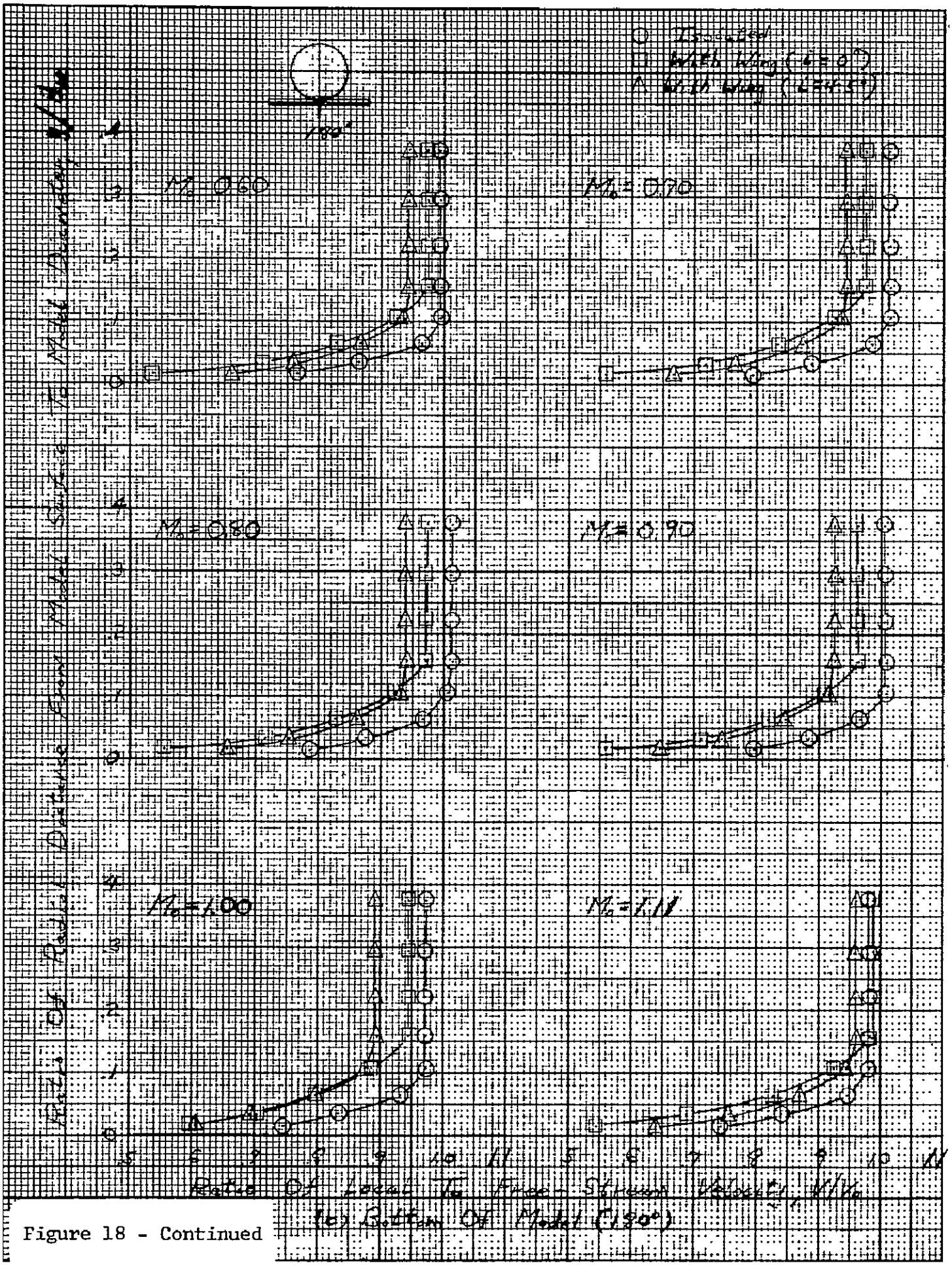

Figure 18 - Continued

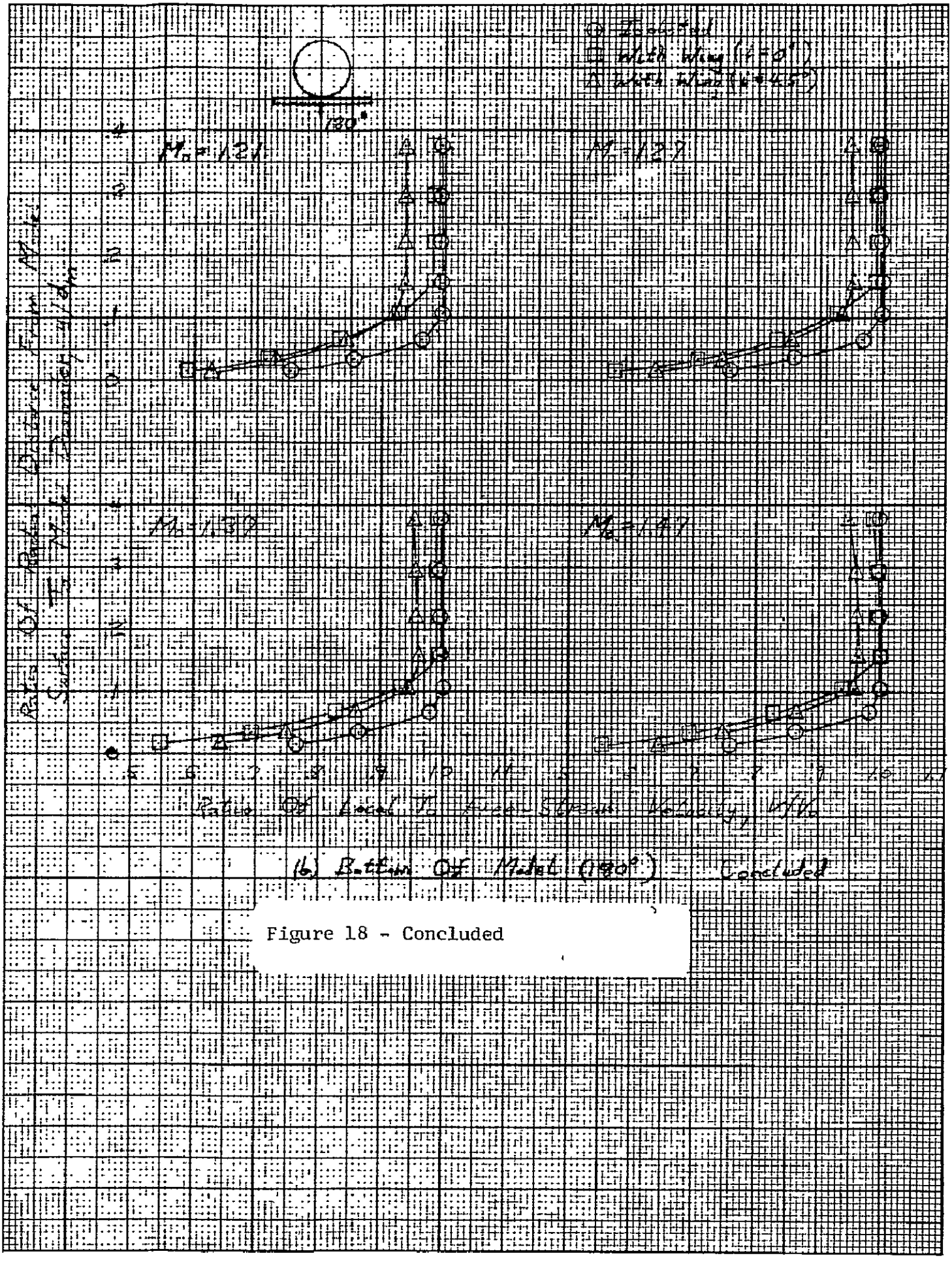

Figure 18 - Concluded

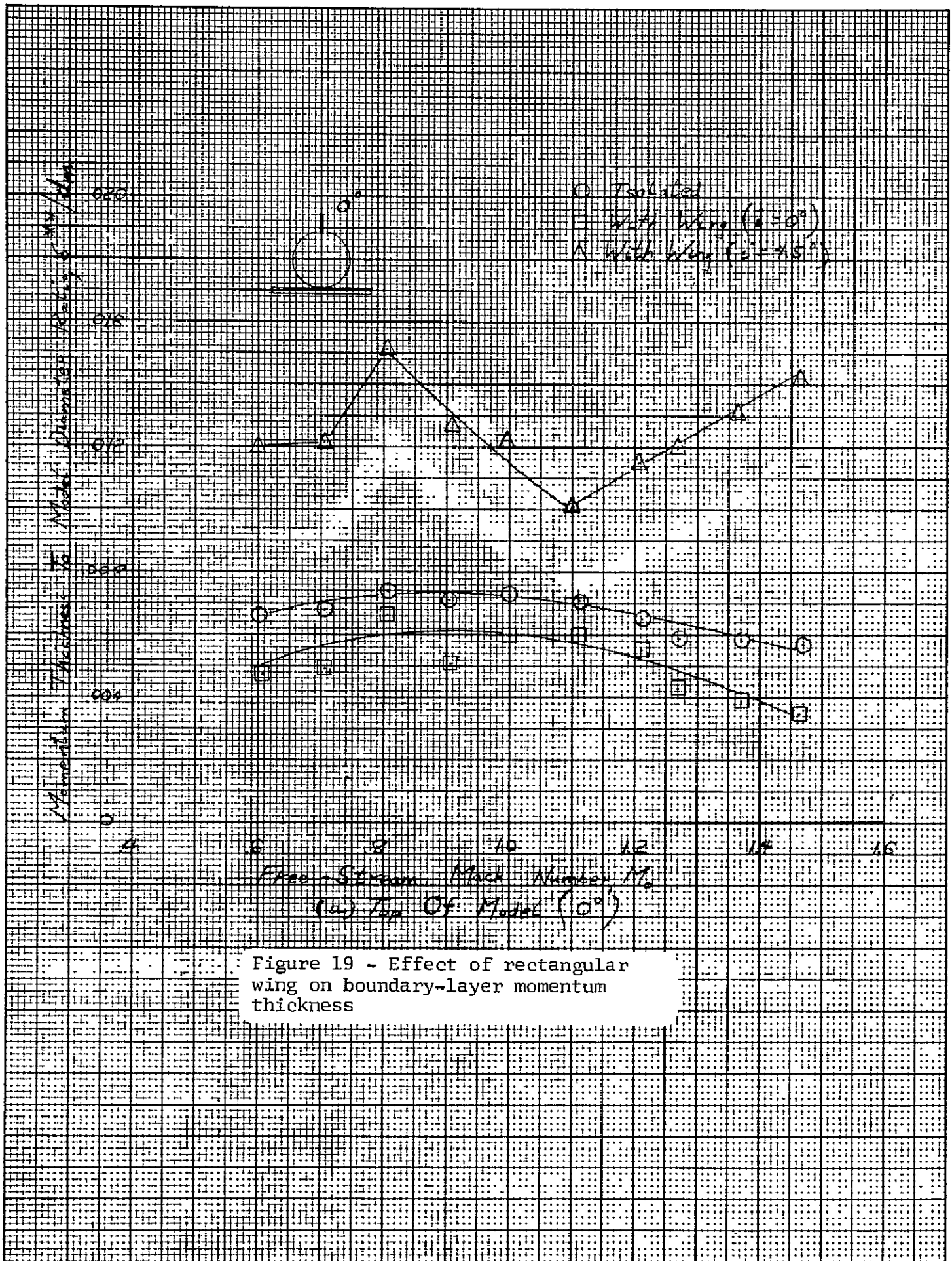

Figure 19 - Effect of rectangular wing on boundary-layer momentum thickness

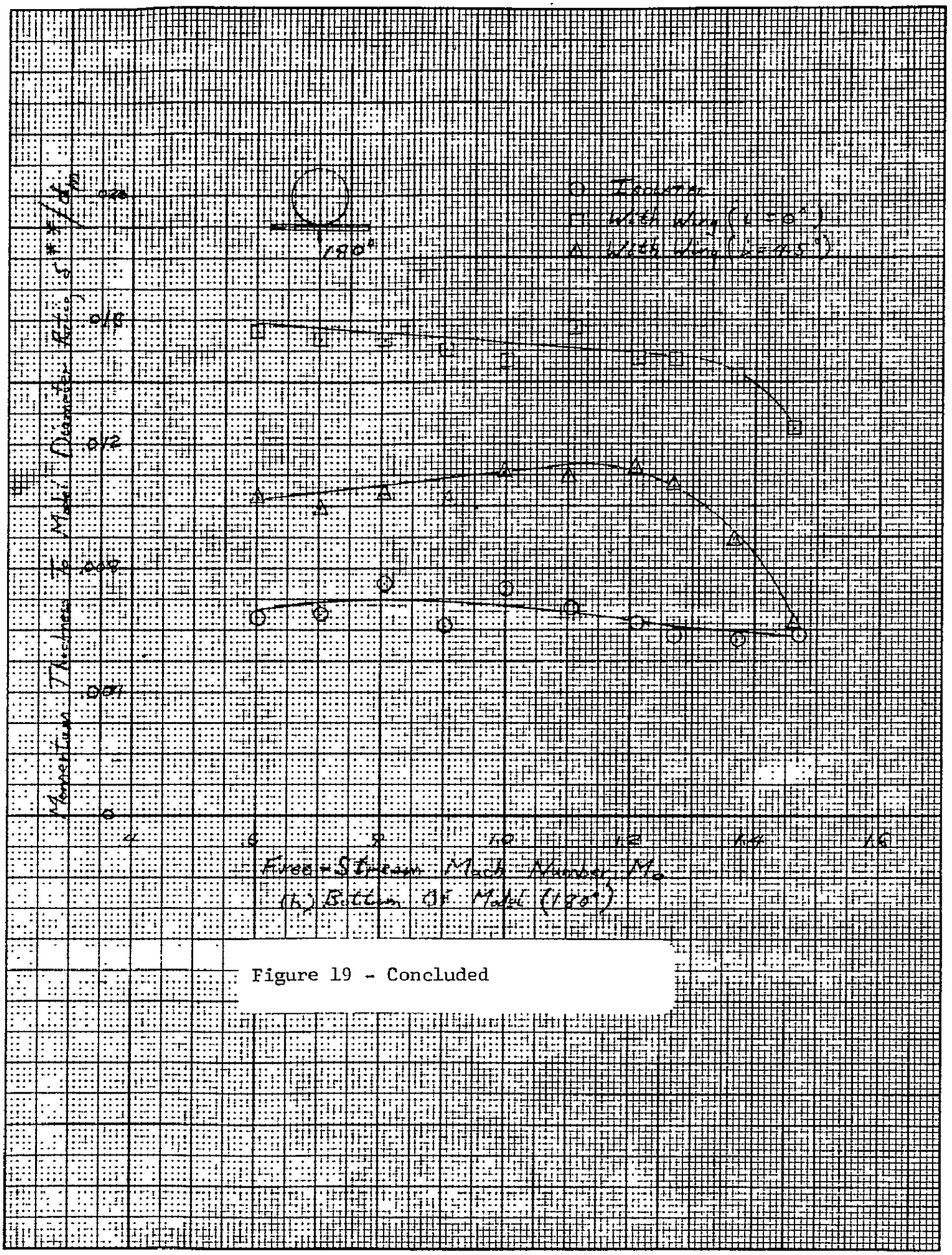

Figure 19 - Concluded